Journal of Glaciology



Article

Cite this article: McArthur KRK, Dow CF and Ehrenfeucht S (2026) The impact of the friction law on coupled subglacial hydrology and ice flow modeling. *Journal of Glaciology* **72**, e104, 1–18. https://doi.org/10.1017/jog.2026.10216

Received: 1 October 2025 UTC
Revised: 19 August 2026 UTC
Accepted: 2 September 2026 UTC

Keywords:
glacier hydrology; ice dynamics; ice-sheet modeling; subglacial processes

Corresponding author:
Koi R. K. McArthur;
Email: kr2mcart@uwaterloo.ca

© The Author(s), 2026. Published by Cambridge University Press on behalf of International Glaciological Society. This is an Open Access article, distributed under the terms of the Creative Commons Attribution-NonCommercial-ShareAlike licence (http://creativecommons.org/licenses/by-nc-sa/4.0), which permits non-commercial re-use, distribution, and reproduction in any medium, provided the same Creative Commons licence is used to distribute the re-used or adapted article and the original article is properly cited. The written permission of Cambridge University Press or the rights holder(s) must be obtained prior to any commercial use.

The impact of the friction law on coupled subglacial hydrology and ice flow modeling

Koi R. K. McArthur[1], Christine F. Dow[2] and Shivani Ehrenfeucht[3]

[1]Department of Applied Mathematics, University of Waterloo, Waterloo, ON, Canada; [2]Department of Geography and Environmental Management, University of Waterloo, Waterloo, ON, Canada and [3]Earth System Analysis, Potsdam Institute for Climate Impact Research (PIK), Potsdam, Germany

Abstract

Basal sliding is an important component of ice motion that is integrated into ice flow models via the use of a friction law, which relates basal shear stress to basal sliding speed and effective pressure. Recent two-way model coupling has utilized temporally changing effective pressure from subglacial hydrology models to drive ice dynamics models. However, there is still significant work required to understand how the friction law impacts such two-way coupled models. Here, we use the Siple Coast, West Antarctica, as a case study to examine these impacts. We compare the Budd and Schoof friction laws, as well as two new regularized Coulomb friction laws that we propose, which respond to changes in ice speed and effective pressure in a way that is consistent with subglacial conditions predicted from subglacial hydrology modeling. We find that the Budd and Schoof friction laws struggle to operate with two-way coupled modeling, leading to a non-physically large speedup of ice in the interior of the ice sheet. Instead, the new friction laws that we propose do not lead to such instabilities in ice motion, producing more physically realistic ice flow outputs.

Introduction

Basal sliding is a key component of ice dynamics and plays an important role in the motion of fast flowing regions of ice (Engelhardt and Kamb, 1998). It is incorporated into ice flow models via the use of a sliding law or a friction law, which relates the basal shear stress to the basal sliding speed and other quantities thought to be relevant to the basal shear stress, such as the effective pressure (difference between ice overburden pressure and subglacial water pressure). Recent developments in subglacial hydrology modeling have opened the door for the improved representation of basal conditions in ice-sheet modeling through the development of two-way coupled models, where the effective pressure in the friction law is taken from the subglacial hydrology model. These models have been applied at the catchment scale in both the Greenland and Antarctic ice sheets (Cook and others, 2022; Pelle and others, 2024; Sommers and others, 2024; Meyer and others, 2026). However, while the representation of a temporally variable subglacial drainage system rests on stronger theoretical ground than models that assume temporally constant effective pressure, it also results in amplification of inaccuracies in the subglacial hydrology model and the basal friction law, the latter of which was designed for temporally constant effective pressure. For this reason, the adoption of two-way coupled models by the glaciological community will be inhibited by flaws in both subglacial hydrology models and friction laws.

One significant limitation with two-way coupled models is that they use two independent descriptions of the subglacial system, one from the friction law and one from the subglacial hydrology model. For these two-way coupled models to become useful, it is necessary to develop a description of subglacial conditions unified between the friction law and the subglacial hydrology model. One approach to achieving this is through altering the subglacial hydrology model, applied by Gilbert and others (2022) and Togaibekov and others (2024). Here, we focus on an alternative approach, unifying the description of basal conditions between the subglacial hydrology model and friction law by directly changing the friction law.

Friction laws

One of the early sliding laws is the Weertman sliding law (Weertman, 1957) given by

$$\tau_b = C_w^2 \, |\vec{u_b}|^{s-1} \, \vec{u_b}, \tag{1}$$

Downloaded from https://www.cambridge.org/core. 19 Nov 2026 at 14:02:16, subject to the Cambridge Core terms of use.

where τ_b is the basal shear stress, C_w is the Weertman friction coefficient, $\vec{u_b}$ is the basal ice velocity and s is a friction law exponent. Weertman (1957) developed this sliding law by considering the flow of ice due to regelation and enhanced creep over cubic bedrock protrusions, and determined that C_w was dependent on the ratio of the size of the bedrock protrusions to their spacing.

Shortly after, Lliboutry (1959) proposed a friction law that, along with regelation and viscous creep, considered water filled cavitation in the lee of bedrock obstacles. The inclusion of cavitation resulted in a basal shear stress with an effective pressure dependence. Lliboutry and Weertman would continue to refine their theories of sliding throughout the 1960s (Lliboutry, 1968), but from these advances, only the original law proposed by Weertman (1957) is widely used today (Fowler, 2010). However, later studies would continue to find evidence supporting effective pressure dependence of the basal shear stress. Through laboratory experiments, Budd and others (1979) proposed the Budd sliding law, given by

$$\tau_b = C_b^2 N^r \, |\vec{u_b}|^{s-1} \, \vec{u_b}, \tag{2}$$

where N is the effective pressure, and r is a positive friction law exponent. The Budd sliding law is a power law that is also commonly used in ice-sheet modeling studies today.

Iken (1981) found that, for a glacier bed modeled after a tilted staircase, there is a maximum ratio of the basal shear stress to the effective pressure. This ratio is equal to the maximum angle on the stoss side of bedrock protrusions and is known as Iken's bound ($C_{\max}$). Schoof (2005) extended this result to a general bedrock geometry and modeled sliding over a linked cavity system assuming a linear ice rheology. For low ice speed and high effective pressure, the basal shear stress was proportional to the ice speed, and for low effective pressure and high ice speed the bounded nature of the basal shear stress was observed. Schoof (2005) developed a friction law with the qualitative aspects of his findings, acting like the Weertman sliding law for high effective pressure and low ice speed, and having $\tau_b \approx C_{\max} N$ for low effective pressure and high ice speed. This type of friction law has a continuous transition between Weertman and Coulomb sliding and is known as a regularized Coulomb friction law.

Finally, based on results using a nonlinear ice rheology to model sliding over sinusoidal and ellipsoidal bedrock protrusions, Gagliardini and others (2007) suggested friction laws should follow the following set of conditions:

(1) $(\frac{\tau_b}{CN})^n = f(\chi)$, where $\chi = \frac{u_b}{C^n N^n A_s}$, C is a parameter which is less than or equal to $C_{\max}$, A_s relates the basal shear stress to the basal sliding speed in the limit there is no cavitation (Weertman sliding), and n is the exponent in Glen's flow law (Glen and Perutz, 1955);
(2) $\left|\frac{\partial f}{\partial \chi}\right|_{\chi=0} = 1$ (i.e. when $\chi = 0, f(\chi)$ is tangent to χ);
(3) $f(\chi = \chi_m) = 1$ where $\frac{\partial f}{\partial \chi} = 0$ (i.e. $f(\chi) = 1$ at the maximum, where $\chi = \chi_m$);
(4) $\tau_b \leq N C_{\max}$ for all $\chi > \chi_m$.

The first condition specifies how the basal shear stress, the basal sliding speed and the effective pressure can be related to each other. The second condition ensures that in the limit that there is no cavitation at the glacier bed (when $\chi = 0$, $u_b = 0$, so there is no cavitation because there is no sliding), the friction law behaves like the Weertman sliding law. The third and fourth conditions enforce Iken's bound. From these four conditions, they proposed a friction law given by

$$\frac{\tau_b}{N} = C \left(\frac{\chi}{1 + \alpha \chi^q} \right)^{1/n}, \quad \alpha = \frac{(q-1)^{(q-1)}}{q^q}, \tag{3}$$

where q is a parameter of the friction law that controls the rate at which τ_b / N decreases after reaching χ_m.

Coupled models

To use a sliding law or a friction law in an ice flow model, values of the friction law exponents, the basal friction coefficient, the basal sliding velocity and in some cases the effective pressure must be determined. The friction law exponents are typically taken to be spatially uniform and temporally constant, and the basal sliding velocity comes from the ice flow model itself. When modeling real domains, the basal friction coefficient is typically solved for using inverse methods, so that the modeled ice velocity matches well with observations of surface velocity at the start of the simulation (MacAyeal, 1993; Morlighem and others, 2013). Observations such as ice surface elevation can be equivalently used in place of or in conjunction with the ice surface velocity (Joughin and others, 2019). The effective pressure is difficult to measure using geophysical observations, and it changes over time (Covington and others, 2020), particularly in regions where there is surface melt reaching the base of the ice. Therefore, the effective pressure used in ice flow models is either parameterized or taken from the output of a subglacial hydrology model (McArthur and others, 2023), which leads to the possibility of coupled models.

Hard-bed subglacial hydrologic systems have been observed to exhibit a variety of drainage configurations, with the ability for self-organizing large drainage channels to form in some glaciers. The characteristics of the subglacial drainage system vary through space and time and have a history of being represented by connected efficient or inefficient components to approximate these changes in flow regime. Inefficient drainage is conceptualized as a system of cavities linked together through narrow orifices, known as a linked cavity system (Walder, 1986; Kamb, 1987), while efficient drainage is represented by a network of linked R-channels (Röthlisberger, 1972), which are incised into basal ice. The most sophisticated hard-bed subglacial hydrology models are solved over two-dimensional (2-D) domains and can model both efficient and inefficient drainage. The Glacier Drainage System (Werder and others, 2013, GlaDS) model is solved using finite element methods; each element surface represents a linked cavity system, which is connected to an R-channel that evolves on each element edge. Where drainage is inefficient, channel cross-sectional area will remain close to zero. The Subglacial Hydrology and Kinetic, Transient Interactions (Sommers and others, 2018, SHAKTI) model is also solved over two dimensions using finite element methods. Unlike GlaDS, SHAKTI does not directly model R-channels, but has a water discharge that is parameterized as a function of the Reynolds number, which leads to efficiently flowing elements with higher average gap height that represent R-channel behavior.

The friction laws and subglacial hydrology models discussed so far have focused on hard-bed systems. Although there has been substantial work regarding soft bed friction (Iverson and others, 1998; Zoet and Iverson, 2020) and subglacial hydrology (Walder and Fowler, 1994; Tulaczyk and others, 2000; Flowers and Clarke, 2002a, 2002b; Bougamont and others, 2011, 2015), ice-sheet models running over large domains often use hard bed sliding laws

Downloaded from https://www.cambridge.org/core. 19 Nov 2026 at 14:02:16, subject to the Cambridge Core terms of use.

(Seroussi and others, 2020), and hard-bed subglacial hydrology models have been applied at the ice-sheet scale (Ehrenfeucht and others, 2025). Furthermore, soft-bed friction exhibits a range of behavior that is mathematically similar to that of hard-bed friction in both slow (Zoet and Iverson, 2020) and fast (Iverson and others, 1998) flowing regions, suggesting the applicability of regularized Coulomb friction laws to soft-bed systems. Despite the differences in actual mechanisms by which water is routed and stored in a soft-bed system, soft-bed subglacial hydrology exhibits the same underlying principals as hard-bed hydrology, where ice geometry drives drainage and water is stored locally. For these reasons, we focus entirely on hard-bed friction and subglacial hydrology modeling and further discuss the applicability of these modeling choices to soft-bed systems in the Supplementary Material Text S1.

Effective pressure outputs from hard-bed subglacial hydrology models have been applied in the friction laws of ice flow models. In some cases, this has taken the form of one-way coupling in both Greenland and Antarctica, where GlaDS and SHAKTI are run to steady state, and then the effective pressure is used in an ice flow model (Ehrenfeucht and others, 2023; Zhao and others, 2025). However, two-way coupled models have also been applied to the ice sheets, where effective pressure from the subglacial hydrology model is input to the friction law of the ice flow model and the evolving glacier geometry and velocity from the ice flow model is, in turn, input into the subglacial hydrology model (Cook and others, 2022; Pelle and others, 2024; Sommers and others, 2024; Meyer and others, 2026; McArthur and others, 2026a). There have also been several studies applying two-way coupling to synthetic domains (Hewitt, 2013; Hoffman and Price, 2014; Gagliardini and Werder, 2018; Lu and Kingslake, 2024), not necessarily with GlaDS or SHAKTI. However, most two-way coupled models to date use two independent descriptions of subglacial conditions, one from the friction law and one from the subglacial hydrology model. So, it is possible that for a friction law that describes fast flow, the subglacial hydrology model predicts low cavitation, and for a friction law that describes slow flow, the subglacial hydrology model predicts high cavitation. Instead, Gilbert and others (2022) developed a 'hydraulically consistent' framework for describing subglacial conditions, which formulates the friction law and subglacial hydrology model (they used a version of GlaDS) in terms of a shared 'cavitation state'. However, this framework has only been applied to alpine glaciers (Gilbert and others, 2022; Togaibekov and others, 2024), and the reformulated subglacial hydrology model strays from the original from Werder and others (2013) to better match observations of glacier velocity.

The goal of the work here is to analyze the impact of the friction law on two-way coupled ice flow/subglacial hydrology models, using a two-way coupled modeling setup with GlaDS and the Ice-sheet and Sea-level System Model (Larour and others, 2012, ISSM) applied to the Siple Coast, West Antarctica, as a case study to aid our analysis. We use various friction laws in the coupled model, including the Budd sliding law, a version of the friction law from Eqn (3) that is commonly known as the 'Schoof friction law', and two regularized Coulomb friction laws that we propose specifically for two-way coupled modeling, which like Gilbert and others (2022) and Togaibekov and others (2024), have a description of basal conditions unified between the friction law and subglacial hydrology model. We additionally test the impact of these friction laws for one-way vs two-way coupled modeling by running the corresponding ice flow models with each of the mentioned friction laws.

Methods

Study area

The Siple Coast in West Antarctica houses topographically unconstrained ice streams that stagnate and reactivate on timescales of multiple centuries (Catania and others, 2012). These changes in ice motion are thought to be the result of internal ice-sheet dynamics, including changes in the basal conditions of the ice sheet such as the evolution of the subglacial hydrologic system (Beem and others, 2014). The Siple Coast ice streams are underlain with a water-saturated till layer that is close to ice overburden pressure (Blankenship and others, 1986; Engelhardt and others, 1990). A mix of fast and slow flowing regions, combined with the characteristic low effective pressure of the Siple Coast ice streams make the Siple Coast an ideal study site for investigating the impact of the friction law on coupled modeling. For example, low effective pressure ensures effective pressure relevance in regularized Coulomb friction laws.

The model domain consists of the combination of the Ross Ice Shelf and the Ross Sea subglacial hydrologic catchment, computed by assuming that water flows in the direction of the negative gradient of overburden hydraulic potential. This is equivalent to assuming flow with a spatially uniform effective pressure. As we do not have estimates of effective pressure prior to running a subglacial hydrology model, this assumption of spatial uniformity or another effective pressure parameterization is necessary to determine a domain boundary. The initial steady-state subglacial hydrology run described in the model initialization section does not have water amalgamation at the domain boundary while using a zero flux boundary condition, suggesting that the assumption of uniform effective pressure was a good approximation for determining the domain boundary. The computational mesh consists of 429 316 elements with a minimum edge length of 225 m. The mesh has a typical edge length of 10 km but is refined near the troughs draining through the Transantarctic Mountains, in the Ross Ice Shelf, in the Lake Vostok area and in areas where ice speed from MEaSUREs v2 (Rignot and others, 2017) is $> 100\,\mathrm{m\,a^{-1}}$.

Ice velocity from MEaSUREs v2 (Rignot and others, 2017), and bed topography and ice thickness from BedMachine Antarctica v3.4 (Morlighem and others, 2020) over the model domain are shown in Fig. 1. The fast flowing ice streams of the Siple Coast are clearly visible in Fig. 1a, draining into the Ross Ice Shelf from the West. These ice streams have minimal topographic control, with bed elevation change on the order of a couple of hundred meters from trunk to ridge (Fig. 1b), with local deeper depressions within the beds of the ice streams not resulting in locally faster flow (Fig. 1a,b).

Subglacial hydrology model

We use GlaDS, implemented in ISSM, with a small change to the sheet equations that describe the linked cavity system. The hydrology sheet evolves as

$$\frac{\partial h}{\partial t} = \omega_s - \nu_s \tag{4}$$

$$\omega_s = \begin{cases} u_b(h_r - h)/\ell_r & h < h_r \\ 0 & h \geq h_r \end{cases}, \tag{5}$$

$$\nu_s = \tilde{A} h \, |N|^{n-1} N, \tag{6}$$

Downloaded from https://www.cambridge.org/core. 19 Nov 2026 at 14:02:16, subject to the Cambridge Core terms of use.

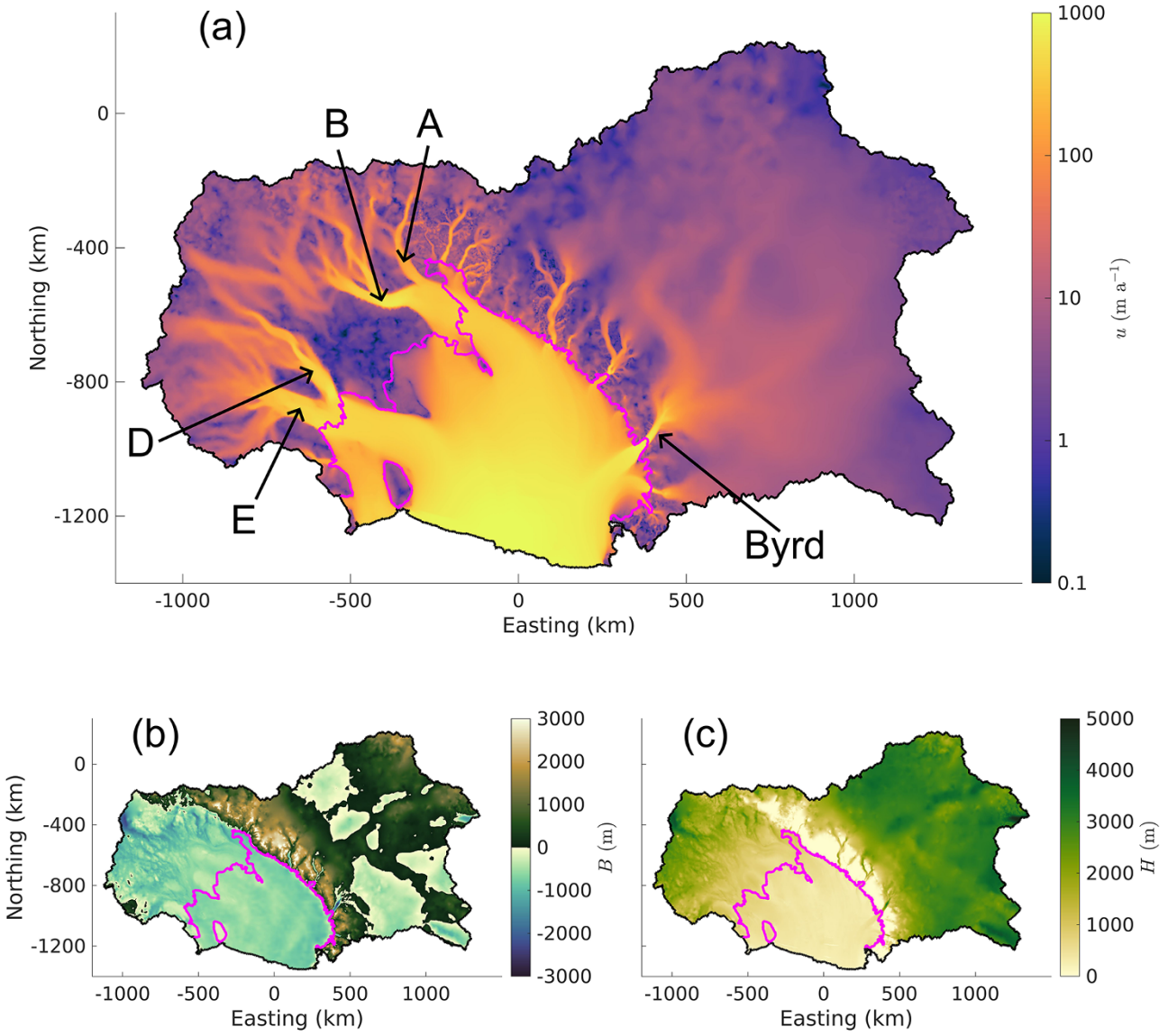


Figure 1. Ross Sea subglacial hydrologic catchment and Ross Ice Shelf ice speed, bed topography and ice thickness. (a) is ice speed from MEaSUREs v2 (Rignot and others, 2011, 2017; Mouginot and others, 2012, 2017), with Ice Streams A, B, D and E, and Byrd Glacier labeled. (b) is bed topography from BedMachine Antarctica v3.4 (Morlighem and others, 2020), and (c) is ice thickness from BedMachine Antarctica v3.4 (Morlighem and others, 2020). The pink lines represent the grounding line. Northing and Easting in all figures are from WGS 84/Antarctic polar stereographic coordinates referenced to the 71° S latitude.

$$N = \begin{cases} \phi_0 - \phi + \rho_w g h & h < h_c \\ \phi_0 - \phi + \rho_w g h \cdot \exp\left(\gamma(\frac{h-h_c}{h_c})\right) & h \geq h_c \end{cases}, \quad (7)$$

where h is the hydrology sheet thickness, ω_s is the hydrology sheet opening rate, ν_s is the hydrology sheet closing rate, u_b is the basal ice speed, h_r is the typical bedrock bump height, ℓ_r is the typical cavity spacing, $\tilde{A}$ is the ice rheological constant multiplied by an order one factor $(2/n^n)$ related to cavity geometry (semi-cylinder), N is the effective pressure, $\phi_0 = \rho_w g B + p_i$ is the overburden hydraulic potential, ρ_w is the density of freshwater, g is the gravitational acceleration, B is the bed elevation, p_i is the ice overburden pressure, $\phi = \rho_w g B + p_w$ is the hydraulic potential, p_w is the water pressure, and h_c and γ are constants controlling the growth of subglacial lakes. Water is routed in the direction of the negative hydraulic potential gradient; therefore, changes in water pressure drive the evolution of flow through the distributed system. Subglacial lakes form when $h \geq h_r$ and fill due to the closing rate term, which becomes negative when the effective pressure becomes negative. Lake depth reaches steady state when $N = 0$. For $h < h_c$, the effective pressure is calculated by taking the subglacial water pressure at the water surface. However, GlaDS sometimes produces areas with large hydraulic potential lows, so to prevent the runaway growth of subglacial lake depth we allow the effective pressure to exponentially increase as a function of lake depth for $h \geq h_c$. In reality, a system where $\phi > \phi_0$ would result in a visco-elastic response of the ice sheet, which would spread water away from the subglacial lake. GlaDS lacks such a mechanism and our exponential increase in effective pressure is meant to spread water away from these hydraulic potential lows in the absence of such a visco-elastic mechanism. A detailed description of the full GlaDS equations, including the channel equations, which we do not alter, can be found in Werder and others (2013).

Downloaded from https://www.cambridge.org/core. 19 Nov 2026 at 14:02:16, subject to the Cambridge Core terms of use.

Table 1. Table of relevant parameters.

Parameter	Value	Units
Bedrock bump height (h_r)	0.08	m
Cavity spacing (ℓ_r)	2	m
Channel conductivity (k_c)	5×10^{-2}	$m^{3/2}\,kg^{-1/2}$
Coupling strength constant (ζ)	10^7, 2×10^7	$m^{-4}\,kg\,s$
Coupling strength constant (α)	10^{22}	$m^{-4}\,kg^3\,s^{-5}$
Start exponential fill thickness (h_c)	100, 10	m
Englacial void ratio (e_v)	10^{-5}	
Exponential fill exponent (γ)	$\ln(10)$	
First channel flow exponent (α_c)	5/4	
First sheet flow exponent (α_s)	5/4	
Freshwater density (ρ_w)	1000	$kg\,m^{-3}$
Friction exponent (m)	1/3	
Glen's flow constant (n)	3	
Gravitational acceleration (g)	9.81	$m\,s^{-2}$
Ice density (ρ_i)	910	$kg\,m^{-3}$
Ice flow constant in GlaDS ($\tilde{A}$)	2.5×10^{-25}	$Pa^3\,s^{-1}$
Iken's bound (C_{max})	0.5	
Maximum channel area	500	m^2
Pressure melt coefficient (c_t)	7.5×10^{-8}	$K\,Pa^{-1}$
Second sheet flow exponent (β_s)	3/2	
Second channel flow exponent (β_c)	3/2	
Sheet conductivity (k_s)	10^{-3}	$m^{7/4}\,kg^{-1/2}$
Sheet width below channel (ℓ_c)	2	m
Seawater density (ρ_{sw})	1023	$kg\,m^{-3}$

GlaDS requires inputs of ice velocity, glacier geometry and basal melt rate. For all runs, melt water is taken from the initMIP Antarctica ISSM Control run final time step (Seroussi and others, 2019). During the initialization procedure (outlined in more detail below) when GlaDS is run uncoupled to steady state, ice velocity is taken from MEaSUREs v2 (Rignot and others, 2017) and glacier geometry is taken from BedMachine Antarctica v3.4 (Morlighem and others, 2020). Following that, ice velocity and glacier geometry are taken from the ice flow model. A zero flux boundary condition is imposed on the domain boundary, and a $\phi = 0$ Dirichlet boundary condition is imposed at the grounding line.

Table 1 provides a list of parameters used in GlaDS. GlaDS has a history of application in Antarctica (Dow and others, 2020, 2022; McArthur and others, 2023; Pelle and others, 2024; Ehrenfeucht and others, 2025), and parameter values remain similar across these studies. This informs our choice of model parameters here, except for the sheet conductivity (k_s), which is tuned to produce realistic water pressure (generally close to overburden pressure but without large areas above overburden pressure) for this domain. A value of $k_s = 10^{-3}\,m^{7/4}\,kg^{-1/2}$ is used in our study, as lower values of the sheet conductivity lead to large areas of negative effective pressure in the initialization procedure. Effective pressure outputs from alternative sheet conductivity values as well as a more detailed discussion on GlaDS parameter choices can be found in the Supplementary Material Text S2. Further details on GlaDS parameters can be found in Werder and others (2013).

Ice flow model

The ice flow model consists of a stress balance model and a mass transport model implemented in ISSM. For the stress balance model, we use the 2-D shallow shelf approximation (MacAyeal 1989, SSA), which includes the basal shear stress as its own term in the balancing equation, as opposed to imposing it as a basal boundary condition as in a three-dimensional (3-D) model. The basal shear stress is calculated from the basal ice speed and the effective pressure using a friction law. We use the depth averaged mass transport model described in Larour and others (2012) to update the ice geometry at each time step. The ice flow model requires inputs of effective pressure, basal friction coefficients and ice rigidity. The effective pressure is taken from GlaDS, and the basal friction coefficient and ice rigidity are determined using inverse methods to match simulated and observed ice surface velocity during the model initialization procedure. The ice flow model is run over the Ross Sea subglacial hydrologic catchment and the Ross Ice Shelf. Dirichlet boundary conditions on the ice velocity and thickness are applied at the domain boundary for stress balance and mass transport respectively. The model domain does not evolve in time, which, in conjunction with the boundary conditions of the stress balance and mass transport models, results in a temporally constant calving rate. The ice mask is allowed to evolve if ice reaches zero thickness in the model.

Friction laws

The basal shear stress is calculated using one of four friction laws: (1) the Budd friction law (Budd and others, 1979); (2) the Schoof friction law (Schoof, 2005; Gagliardini and others, 2007); (3) a version of the Schoof friction law that we have modified, which we refer to as the 'hydrology-modified Schoof friction law'; and (4) a new friction law we propose that acts as a linear combination of Weertman and Coulomb sliding terms, which we refer to as 'the linear combination friction law'. The Schoof friction law is given by

$$\tau_b = \frac{C_s^2\,|\overrightarrow{u_b}|^{m-1}}{(1 + (C_s^2/(C_{\max}N))^{1/m}\,|\overrightarrow{u_b}|)^m}\overrightarrow{u_b}, \tag{8}$$

where C_s is the Schoof friction coefficient, and $m = 1/n$ is a friction law exponent. This is a special case of Eqn (3), where $q = 1$, $C = C_{\max}$ and $A_s = C_s^{-2/n}$. $\xi_s = (C_s^2/(C_{\max}N))^{1/m}\,|\overrightarrow{u_b}|$ can be thought of as a dimensionless parameter in the denominator of the Schoof friction law that controls the 'sliding regime' of the friction law. When $\xi_s \ll 1$ then $\tau_b \approx C_s^2\,|\overrightarrow{u_b}|^{m-1}\,\overrightarrow{u_b}$ and the friction law is in a Weertman sliding regime, and when $\xi_s \gg 1$ then $\tau_b \approx C_{\max}N$ and the friction law is in a Coulomb sliding regime. The sliding regime (ξ_s) therefore depends on the ratio of $C_s^2/C_{\max}$, which varies spatially over the model domain.

The hydrology-modified Schoof friction law is given by

$$\tau_b = \frac{C_h^2\,|\overrightarrow{u_b}|^{m-1}}{(1 + (\zeta/N)^{1/m}\,|\overrightarrow{u_b}|)^m}\overrightarrow{u_b}, \tag{9}$$

where C_h is the hydrology-modified Schoof friction coefficient (equivalent to C_s in the Schoof friction law and C_w in the Weertman friction law), and ζ is the spatially uniform coupling strength parameter that ensures the sliding regime of the friction law is dependent on subglacial conditions related to basal sliding predicted from subglacial hydrology modeling.

We define the degree of cavitation at the glacier bed as

$$\theta = \begin{cases} h/h_r & h < h_r \\ 1 & h \geq h_r \end{cases}. \tag{10}$$

When $\theta \approx 0$ there is no cavitation and we expect the friction law to be in a Weertman sliding regime, and when $\theta \approx 1$ there is sliding over water filled cavities and we expect the friction law to be in a Coulomb sliding regime. Therefore, the degree of cavitation at the glacier bed acts as a proxy for sliding conditions predicted from

Downloaded from https://www.cambridge.org/core. 19 Nov 2026 at 14:02:16, subject to the Cambridge Core terms of use.

subglacial hydrology modeling, and we would expect the sliding regime to be a monotonically increasing function of the degree of cavitation, going to 0 when $\theta = 0$, and going to ∞ when $\theta = 1$. The relationship between ξ and θ should be the same throughout the model domain, so that the sliding regime is consistent with subglacial conditions predicted from the subglacial hydrology model. Throughout the manuscript, we will equivalently say that the sliding regime is 'spatially consistent', with the degree of cavitation. Assuming that the hydrology sheet is in steady state, $h < h_r$ and $N > 0$ we can set the left hand side of Eqn (4) equal to 0 and rearrange to find

$$\frac{u_b}{N^n} = \frac{\tilde{A}\theta\ell_r}{1-\theta}, \tag{11}$$

where we see that since $\tilde{A}$ and ℓ_r are spatially uniform in this study, if we take ζ to be spatially uniform then the sliding regime of the hydrology-modified Schoof friction law ($\xi_h = (\zeta/N)^{1/m}|\overrightarrow{u_b}|$) is spatially consistent with the degree of cavitation at the glacier bed, ξ_h goes to 0 as θ goes to 0, and ξ_h goes to ∞ as θ goes to 1. Equation (11) assumes that sliding is the only mechanism by which cavities can open. In reality, cavities also open by melt from turbulent dissipation of potential energy, and frictional and geothermal heat. However, sliding has been shown to be the dominant opening mechanism in a linked cavity system (Walder, 1986; Kamb, 1987), and Eqn (11) is therefore a reasonable approximation. Furthermore, any region with sufficiently large melt will result in the formation of an R-channel (whose dominant opening mechanism is melt from dissipation of potential energy) and no longer be part of the linked cavity system.

We note that the hydrology-modified Schoof friction law is equivalent to the Schoof friction law when the ratio $C_s^2/C_{\max}$ is spatially uniform. One way to accomplish this is by taking C_s and $C_{\max}$ individually to be spatially uniform. Such an approach is common when applying regularized Coulomb friction laws to synthetic domains with two-way coupling (Hewitt, 2013; Hoffman and Price, 2014; Gagliardini and Werder, 2018; Lu and Kingslake, 2024). However, the application of regularized Coulomb friction laws to non-synthetic domains typically requires spatially heterogeneous friction parameters to match modeled and observed ice velocity. The Coulomb friction parameter (Iken's bound) is typically held spatially uniform, while the Weertman friction parameter (the friction coefficient) is varied. This is common in two-way coupled models (Cook and others, 2022; Pelle and others, 2024), as well as one-way coupled or uncoupled models (Brondex and others, 2019; Ehrenfeucht and others, 2023). However, this means that there is not a data-informed constraint on the Coulomb friction parameter, which should be the relevant parameter in fast flowing regions. By requiring ζ to be spatially uniform in the hydrology-modified Schoof friction law, varying C_h to match modeled and observed ice velocities will simultaneously vary $C_{\max} = C_h^2/\zeta$. Consequently, an appropriate value of Iken's bound can be determined in fast flowing regions of the domain.

The functional form of the hydrology-modified Schoof friction law and the Schoof friction law does not allow for the ability to both choose C_i (C_s for the Schoof friction law and C_h for the hydrology-modified Schoof friction law) and $C_{\max}$ and have a sliding regime dependent on the degree of cavitation at the glacier bed. The Schoof friction law allows for the choice of both C_s and $C_{\max}$ but has a sliding regime that is spatially inconsistent with the degree of cavitation at the glacier bed, whereas the hydrology-modified Schoof friction law has a sliding regime that is spatially consistent with the degree of cavitation at the glacier bed but does not allow for the choice of both C_h and $C_{\max}$. This is in fact true for all friction laws of the form proposed by Gagliardini and others (2007), through condition 1 outlined in the 'Introduction' section. Gagliardini and others (2007) developed their friction law criteria based on simulations of sliding over periodic sinusoidal and ellipsoidal bedrock obstacles. The periodicity of the bed ensured that C and A_s were spatially uniform in their analysis. However, for a nonuniform bed with varying C and A_s, it is apparent that a functional form that differs to that proposed in condition 1 is necessary to independently choose Weertman and Coulomb friction parameters to match simulated and observed ice velocity, while having a sliding regime that is spatially consistent with the degree of cavitation at the glacier bed. As a simple example of a functional form that accomplishes this, we propose the linear combination friction law, which acts as a linear combination of Weertman and Coulomb sliding terms, with coefficients dependent on the explicit sliding regime, which sum to one and determine the relevance of each term. The linear combination friction law is given by

$$\tau_b = C_{\max} N |\overrightarrow{u_b}|^{-1} \overrightarrow{u_b} \left(\frac{\xi_\ell}{1+\xi_\ell}\right) + C_\ell^2 |\overrightarrow{u_b}|^{m-1} \overrightarrow{u_b} \left(\frac{1}{1+\xi_\ell}\right), \tag{12}$$

$$\xi_\ell = \alpha \frac{u_b}{N^n}, \tag{13}$$

where C_ℓ is the friction coefficient of the linear combination friction law, ξ_ℓ is the sliding regime of the linear combination friction law, and α is the coupling strength parameter of the linear combination friction law. α serves the equivalent purpose of ζ^n in the hydrology-modified Schoof friction law, in the sense that it relates u_b/N^n to the sliding regime and controls the sensitivity of the basal shear stress to subglacial hydrologic effects. However, since the linear combination friction law allows for the simultaneous choice of $C_{\max}$ and C_ℓ, the physical meaning of α (with respect to bed roughness and angles at the stoss faces of bedrock obstacles) is lost. We choose a value of α similar to ζ^n in the hydrology-modified Schoof friction law. The linear combination friction law is designed to respond to changes in basal sliding speed and effective pressure in the same way that the Schoof and hydrology-modified Schoof friction law do, in the limit that ξ_i goes to 0 or ∞, where ξ_i is ξ_s for the Schoof friction law and ξ_h for the hydrology-modified Schoof friction law. We acknowledge that the functional form of the linear combination friction law is not derived from a theoretical analysis of basal sliding and first principals. Instead, it is a practical solution to model the evolution of friction on real domains in a way that is consistent with our subglacial hydrology modeling. Future work on specifying the functional form of the friction law while keeping the practical use of said friction law in mind is needed, but beyond the scope of this study.

Finally, for the Budd friction law, we take $r = 1$ and $s = 1/3$ so that we have the same effective pressure dependence as the regularized Coulomb friction laws in a Coulomb sliding regime and the same ice speed dependence as the regularized Coulomb friction laws in a Weertman sliding regime.

Model initialization

We aim to approximate the conditions of the ice sheet in 2010 (the start time of the transient simulations) by using an initialization procedure involving inversions for the basal friction coefficient and ice rigidity, model relaxations and running a thermal model to estimate the ice rigidity over the grounded portion of the domain using an empirical parameterization. The initialization procedure

Downloaded from https://www.cambridge.org/core. 19 Nov 2026 at 14:02:16, subject to the Cambridge Core terms of use.

can be broken into four main steps described below (a flowchart to help understand the initialization procedure is given in the Supplementary Material Text S6).

(1) Estimate the effective pressure: We run GlaDS for 100 a to steady state using observed ice velocity from MEaSUREs v2 (Rignot and others, 2017) and ice geometry from BedMachine Antarctica v3.4 (Morlighem and others, 2020). We start with adaptive timestepping as short as 0.1 days and gradually increase the time step to 0.5 days as the model gets closer to steady state. We test sheet conductivities of $k_s = 10^{-4}\,\mathrm{m}^{7/4}\,\mathrm{kg}^{-1/2}$, $k_s = 10^{-3}\,\mathrm{m}^{7/4}\,\mathrm{kg}^{-1/2}$ and $k_s = 5 \cdot 10^{-3}\,\mathrm{m}^{7/4}\,\mathrm{kg}^{-1/2}$ but choose to proceed with $k_s = 10^{-3}\,\mathrm{m}^{7/4}\,\mathrm{kg}^{-1/2}$, which produced the most realistic effective pressure. The results of these steady-state hydrology runs are discussed in the Supplementary Material Text S3.
(2) Invert for the friction coefficient and ice rigidity: Using the effective pressure from steady-state GlaDS, we perform a series of inversions to determine the hydrology-modified Schoof friction coefficient and the ice rigidity. First, we invert for the ice rigidity over the floating portion of the domain and determine it over the grounded portion of the domain by using an empirical parameterization built into ISSM that relates ice temperature to ice rigidity based on Table 3.4 in Cuffey and Paterson (2010). The ice temperature is obtained by solving a 3-D thermal model (Larour and others, 2012) with 59 6116 elements and five vertical layers, and depth averaging the results. Depth averaging the temperature and computing the ice rigidity will likely lead to a more rigid ice sheet, but as all our models use the same rigidity this is unlikely to affect the comparison of the various friction laws. Parameters for this thermal model are given in Larour and others (2012). A Dirichlet boundary condition of modeled atmosphere temperature from RACMO v2.3 (van Wessem and others, 2023) is applied at the glacier surface, and geothermal heat flux from the Aq1 model (Stål and others, 2020; 2021) is applied as a Neumann boundary condition at the glacier base. Next, the basal shear stress is estimated using the Budd friction law and by inverting for the Budd friction coefficient. This initial inversion for the basal shear stress using the Budd friction law is necessary since the hydrology-modified Schoof friction law requires a good initial estimate of the basal shear stress but the Budd sliding law does not. The ice rigidity over the floating portion of the domain is then inverted for once again. Finally, we convert to the hydrology-modified Schoof friction law by solving for the hydrology-modified Schoof friction coefficient given the basal shear stress from the prior friction inversion, and then invert for the hydrology-modified Schoof friction coefficient.
(3) Relax the models individually: Due to feedbacks between GlaDS and the ice flow model leading to instabilities when relaxed together (e.g. negative effective pressure, hydrology sheet growth and ice speedup), the models must first be relaxed separately. We start by running a 20 a ice flow relaxation using effective pressure from the steady-state GlaDS run, the ice rigidity and friction coefficient from step 2, initial ice velocity from MEaSUREs v2 (Rignot and others, 2017), initial ice geometry from BedMachine Antarctica v3.4 (Morlighem and others, 2020) and 1 day timestepping. We then use the ice geometry from this ice flow relaxation to invert again for the hydrology-modified Schoof friction coefficient and the ice rigidity over the floating portion of the domain. The idea is that, by the end of the ice flow relaxation, the ice velocity and geometry should be close to observed values. The ice flow relaxation is then rerun with the friction coefficient and ice rigidity from these inversions. The final ice geometry and velocity from this second relaxation are then used to initialize a 70 a steady-state GlaDS run, with a switch from 0.2 day timestepping to 0.5 day timestepping at 2 a, and a switch from $h_c = 100$ m to $h_c = 10$ m at 50 a (due to unrealistically large sheet thickness in the coupled models when h_c is not reduced).
(4) Relax the coupled model: Once the models are relaxed individually they can be coupled and run for a final short relaxation. We take the effective pressure from GlaDS and the basal shear stress from the ice flow model in step 3 and we use them to calculate the friction coefficient of the friction law to be used in the transient simulation. We perform final inversions for the friction coefficient and the ice rigidity to ensure a close initial match to observed ice motion and run a 1 year relaxation of the model to be used in the transient simulation. This last relaxation and the transient simulations have 0.5 day timestepping for GlaDS and 14 day timestepping for the ice flow model.

The ice flow model is forced with mean surface mass balance between 1980 and 2010 (Kittel and others, 2021; Kittel, 2021), and basal mass balance from the initMIP-Antarctica control run final time step (Seroussi and others, 2019) over the grounded domain and from Adusumilli and others (2020) over the floating domain.

Two-way coupled model initialization is more complicated than the initialization of one-way coupled or uncoupled models due to the strong dependence of ice flow on the basal shear stress and the strong dependence of the hydraulic potential field on ice geometry. If the ice geometry is not sufficiently relaxed at the start of the transient simulation, this could lead to a subglacial hydrologic response and feedbacks that are forced by the initialization procedure. By first relaxing the models separately, we ensure a relaxed ice-sheet geometry and a relaxed hydraulic potential field for that geometry.

List of experiments

To test the impact of the different friction laws, as well as the impact of two-way coupled vs one-way coupled modeling, we run nine transient simulations (Table 2) from 2010 to 2100 under an SSP5-8.5 surface mass-balance forcing scenario (Kittel and others, 2021; Kittel, 2021). SSP5-8.5 is a high emissions climate scenario resulting in significant global warming and associated climatic impacts. For each of the four friction laws, we run one ice flow-only model and one two-way coupled model. For model-IH and model-CH, we use $\zeta = 10^7\,\mathrm{m}^{-4}\,\mathrm{kg\,s}$, but as part of a sensitivity analysis, we run a second coupled model with the hydrology-modified Schoof friction law (model-CH2), with $\zeta = 2 \cdot 10^7\,\mathrm{m}^{-4}\,\mathrm{kg\,s}$. The results of model-CH2 are discussed in the Supplementary Material Text S4. A list of the experiments with their respective names is given in Table 2.

Results

Ice flow

All ice flow models had similar trends throughout the 90 a simulation (Fig. 2). The Siple Coast ice streams slowed down, except in model-IS, where the northern trunk of Ice Stream B (Whillans) accelerated during the simulation (Fig. 2c). The ice upglacier of Ice Streams A (Mercer), B, D (Bindschadler) and E (MacAyeal)

Downloaded from https://www.cambridge.org/core. 19 Nov 2026 at 14:02:16, subject to the Cambridge Core terms of use.

Table 2. List of experiments.

Model name	Iceflow/coupled	Friction Law
Model-IB	Ice flow	Budd
Model-CB	Coupled	Budd
Model-IS	Ice flow	Schoof
Model-CS	Coupled	Schoof
Model-IH	Ice flow	H-Schoof
Model-CH	Coupled	H-Schoof
Model-CH2	Coupled	H-Schoof
Model-ILC	Ice flow	Linear combination
Model-CLC	Coupled	Linear combination

Note: H-Schoof refers to the hydrology-modified Schoof friction law.

thinned, with more significant thinning of 20–30 m upglacier of Ice Streams A and B, and the region upglacier of the Kamb Ice Stream thickened by 30 m in some places by the end of the simulation. Byrd Glacier accelerated, and the ice downglacier of Byrd, in the Ross Ice Shelf, sped up by $>100\,\mathrm{m\,a^{-1}}$ as a result of poorly constrained ice rigidity and friction. These changes in ice motion in the Siple Coast ice streams and Byrd Glacier propagated into the Ross Ice Shelf. However, the change in ice thickness of the Ross Ice Shelf did not always follow the trends in ice motion, indicating that the Ross Ice Shelf may be more sensitive to surface and basal mass balance forcing than to dynamic processes.

The Budd friction law

Model-CB showcased large speedup events of Ice Stream B and the area upglacier of Ice Stream B, resulting in unrealistically large changes in ice speed and thickness on timescales of decades (Fig. 3). Thinning of ice upglacier of Ice Stream B lowered the hydraulic potential, which drew more water into the region, and consequently, lowered the effective pressure. The reduced effective pressure triggered acceleration of inland ice between 2056.8 and 2059.9 (Fig. 3a,b). By 2059.9, this inland ice was moving $>1000\,\mathrm{m\,a^{-1}}$ faster than in 2058 (maximum speedup from 55.0 to 1494 $\mathrm{m\,a^{-1}}$). This ice speedup propagated through Ice Stream B, which was followed by a significant slowdown to 77.0 $\mathrm{m\,a^{-1}}$ by 2080, far below its starting value of 459 $\mathrm{m\,a^{-1}}$ (note that ice stream speeds, effective pressures and sliding regimes are calculated as an areal average with locations defining the ice streams given in Fig. S3). During this

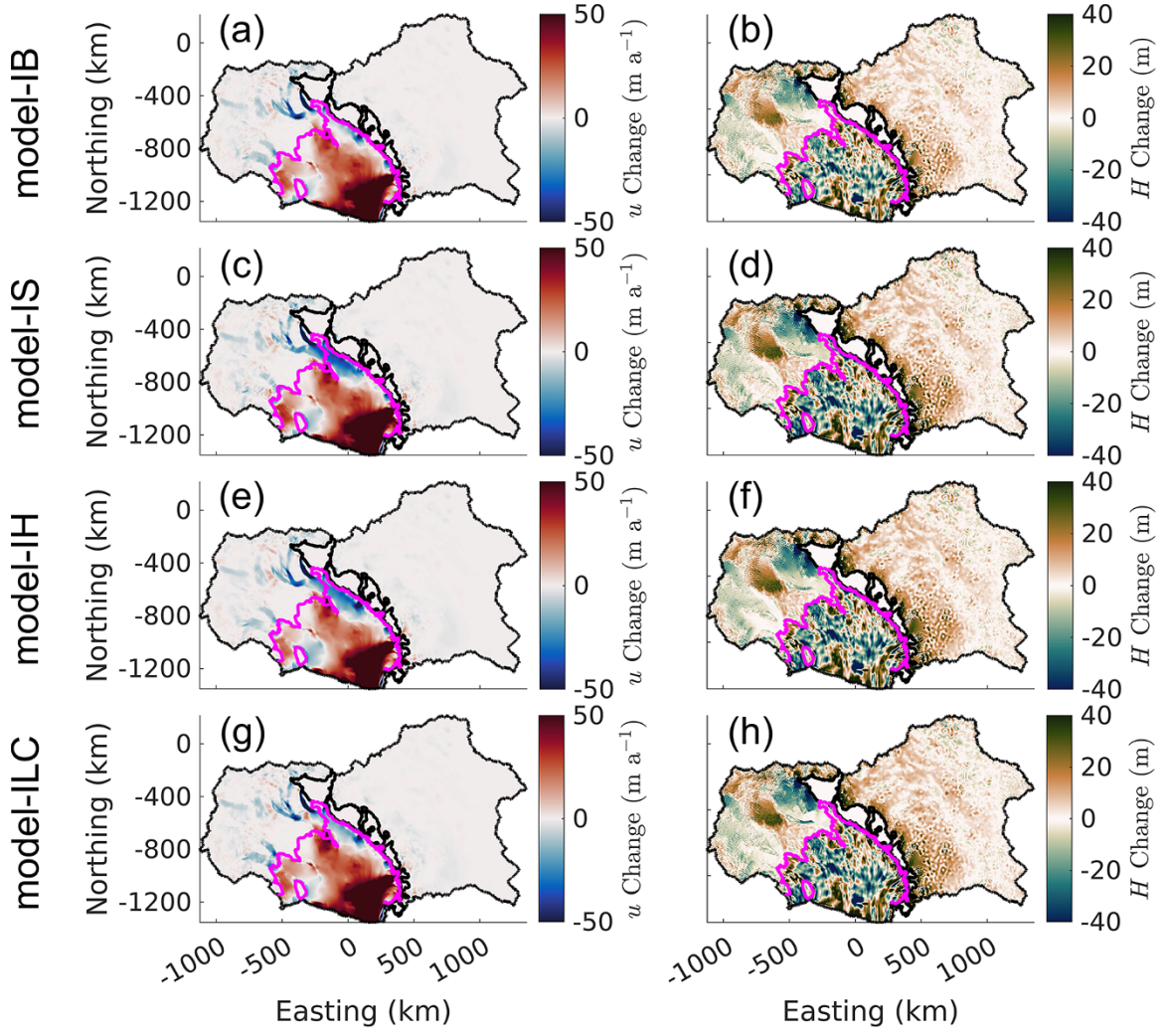


Figure 2. Changes in ice speed and ice thickness for the ice flow models between 2010 and 2100. (a), (c), (e) and (g) show changes in ice speed ($\mathrm{m\,a^{-1}}$) and (b), (d), (f) and (h) are changes in ice thickness (m). The model for each row is named on the left. The pink lines represent the grounding line at the start of the simulation and the black lines represent the domain boundary.

Downloaded from https://www.cambridge.org/core. 19 Nov 2026 at 14:02:16, subject to the Cambridge Core terms of use.

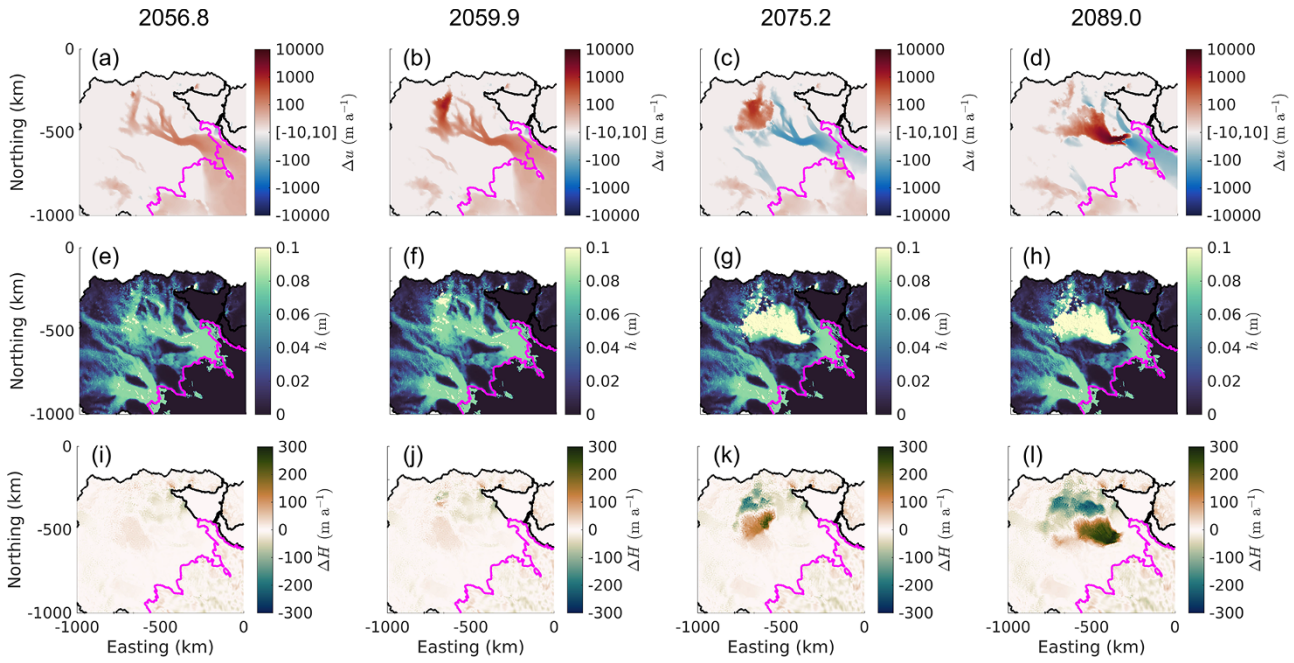


Figure 3. Outputs for model-CB at various points in time. (a)–(d) plot the change in ice speed from the start of the simulation (m a^{-1}); (e)–(h) plot the hydrology sheet thickness (m); and (i)–(l) plot the change in ice thickness relative to the start of the simulation. Pink lines represent the grounding line at the start of the simulation and black lines represent the domain boundary. The simulation time is given above each column. The change in ice speed has a logarithmic scale in the positive and negative direction, with changes with absolute value <10 m a^{-1} in white.

time, when Ice Stream B was decelerating, the subglacial hydrologic system upglacier of Ice Stream B was flooding (hydrology sheet thickness above the typical bedrock bump height) as a result of an extensive hydraulic potential low. The latter was caused by extreme dynamic thinning that occurred following the initial ice speedup event (Fig. 3k). The initial ice speedup event was confined to a faster flowing stream of inland ice, but the expansive hydraulic potential low that it triggered superseded all previous spatial patterns in ice motion (Fig. 3g). This resulted in a large upglacier area of fast moving ice, which funneled into Ice Stream B, increasing in speed to 3318 m a^{-1} ($>$5000 m a^{-1} in some places; Fig. 3d). By the end of the simulation, Ice Streams A and B experienced significant dynamic thickening of $>$200 m in some places, and the region upglacier of Ice Stream B experienced significant dynamic thinning of $>$100 m in some areas (Fig. 3l).

Trends between model-IB and model-CB diverged significantly in the portion of the Siple Coast consisting of Ice Streams A and B. However, these effects were somewhat localized, and trends in Ice Streams D and E were, by comparison, similar between model-IB and model-CB. In model-IB, both these ice streams gradually slowed over the course of the simulation, so that by the end of the simulation ice speed for both ice streams remained within 10 m a^{-1} of their starting values. In model-CB, Ice Stream E sped up by 24.8 m a^{-1} over the course of the simulation, with almost 20 m a^{-1} of this speedup coming within the first 15 a of the simulation. The ice speed variability of Ice Stream E was enhanced in model-CB compared to model-IB, due to changes in the subglacial hydrologic system. In model-CB, Ice Stream D gradually accelerated until mid 2061, where it rapidly slowed by 46.7 m a^{-1} over the next 3 a as a result of the changes to the ice sheet that took place further South in the Ice Stream B area. An ice speedup event of 78.2 m a^{-1} took place over 3 a in the early 2080s, which was also a consequence of changes in the Ice Stream B region.

The Schoof friction law

Much like model-CB, model-CS experienced large speedup events in Ice Stream B. In model-CS, these speedup events reached larger extremes than in model-CB but were confined within a 30 a period between 2040 and 2070 (Fig. 4). Like in model-CB, inland ice upglacier of Ice Stream B thinned at the start of the simulation, resulting in a reduction of effective pressure, particularly in regions of faster flowing ice. The ice stream onset of the southern tributary feeding Ice Stream B accelerated from $<$232.8 m a^{-1} in 2047.6 to 8625 m a^{-1} (maximum speedup) over a span of $<$3 a (Fig. 4b,c), resulting in Ice Stream B reaching a speed of 7102 m a^{-1} (10^4 m a^{-1} in some regions), well above the starting value of 426.6 m a^{-1} (Fig. 4d). The speedup events of model-CS were more extreme than those of model-CB. They were initiated earlier in the simulation than in model-CB, and, unlike in model-CB, they terminated by the end of the simulation. The area upglacier of Ice Streams A and B thinned by $>$100 m in some places, but the ice thickness of the ice streams themselves thinned by $<$50 m, and downstream of Ice Streams A and B, the Whillans Ice Plain thickened by $<$50 m (Fig. 4l).

The hydrology-modified Schoof friction law

As with the coupled models already discussed—model-CB and model-CS—the ice upglacier of Ice Stream B thinned at the start of model-CH. This thinning resulted in a hydraulic potential low and flooding of the subglacial hydrologic system. However, there was no inland ice speedup, despite lower effective pressure. Ice Stream B sped up twice throughout model-CH. In 2063, it increased speed by 52.2 m a^{-1} in just over 4.5 a, and in 2080 it increased speed by 66 m a^{-1} in a similar time frame (Fig. 5d). These speedup events were followed by the slowdown of the ice stream, so that by the

Downloaded from https://www.cambridge.org/core. 19 Nov 2026 at 14:02:16, subject to the Cambridge Core terms of use.

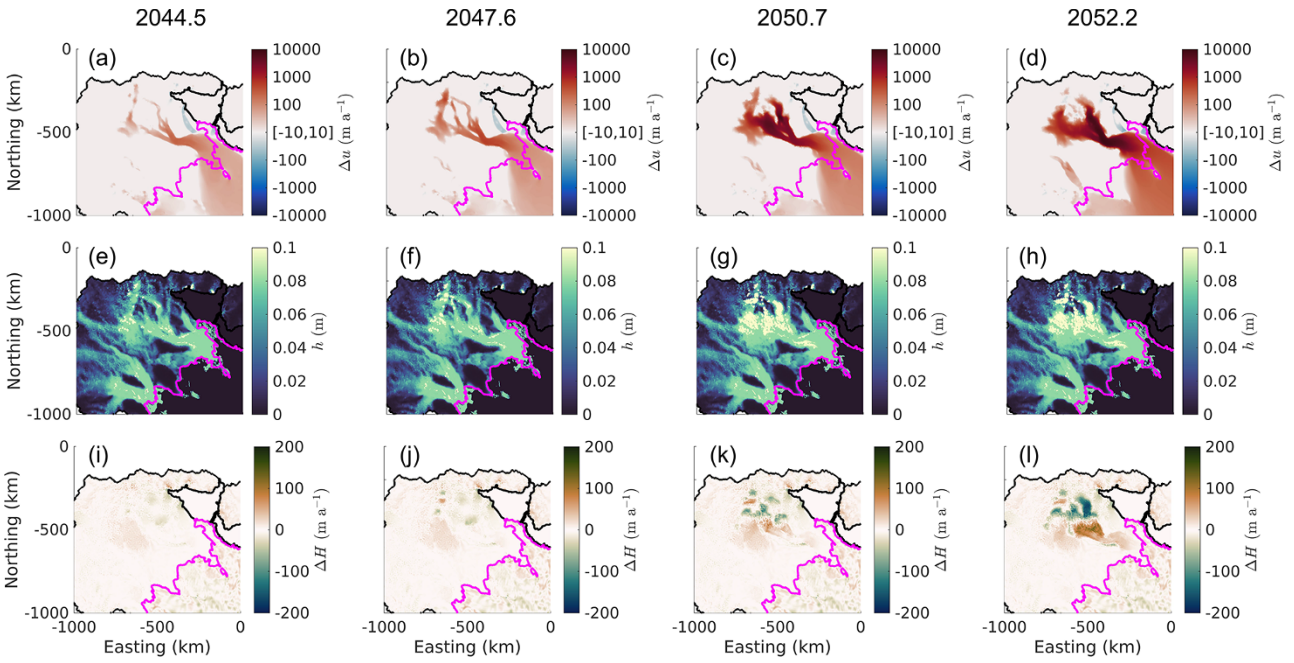


Figure 4. Outputs for model-CS at various points in time. (a)–(d) plot the change in ice speed from the start of the simulation (m a^{-1}); (e)–(h) plot the hydrology sheet thickness (m); (i)–(l) plot the change in ice thickness relative to the start of the simulation. Pink lines represent the grounding line at the start of the simulation and black lines represent the domain boundary. The simulation time is given above each column. The change in ice speed has a logarithmic scale in the positive and negative direction, with changes with absolute value <10 m a^{-1} in white.

end of the simulation, Ice Stream B was 28.8 m a^{-1} slower than its starting speed. The lack of ice acceleration upglacier of Ice Stream B means that dynamic thinning did not occur, and the flooding of the subglacial hydrologic system upglacier in Ice Stream B was not as expansive as it was in model-CB and model-CS. As in model-CB and model-CS, Ice Stream D was affected by the motion of Ice Stream B. However, since the motion of Ice Stream B is much less affected in model-CH than in model-CB and model-CS, the response of Ice Stream D was reduced in model-CH. In fact, only one of the speedup events of Ice Stream B registered in the ice speed trend of Ice Stream D, and it did so as a 4.54 m a^{-1} increase in ice speed. Aside from this small pulse in ice motion experienced in Ice Stream D in model-CH, trends in ice motion for Ice Streams D and E for model-IH and model-CH stayed within 2 m a^{-1} of each other.

As expected, the initial sliding regime of the hydrology-modified Schoof friction law in model-CH aligns with patterns in the initial hydrology sheet thickness. However, the sliding regime of the Schoof friction law in model-CS does not follow these patterns, and areas where hydrology sheet thickness is close to the typical bedrock bump height (implying low effective pressure) have Weertman sliding regimes ($\xi_s < 10^{-10}$). Areas that have low hydrology sheet thickness match more closely between model-CS and model-CH, with model-CS typically classifying these regions as more Coulomb than model-CH. The higher sliding regime of model-CS in these slow moving regions allowed for large changes in the basal shear stress as the subglacial hydrologic system flooded, causing the inland speedup events in model-CS that did not occur in model-CH.

The trend in the logarithm of the sliding regime of Ice Stream B follows very closely to the negative of the trend of the ratio of effective pressure to ice pressure in model-CH (Fig. 5e). Specifically, the correlation between the ratio of effective pressure to ice pressure and the logarithm of the sliding regime is −0.992 in this region. When effective pressure does not vary, as in model-IH, the sliding regime remains nearly constant (Fig. 5f), showcasing the importance of the effective pressure in the evolution of the basal shear stress. In model-CS, there is still a high negative correlation between the logarithm of the sliding regime and the ratio of the effective pressure to ice pressure (−0.861), but it is not as extreme as in model-CH. In model-CS, large changes in ice speed have an impact on the sliding regime, which is in part responsible for the less significant correlation.

The linear combination friction law

The ice speedup events of Ice Stream B in model-CLC were comparable in scale to model-CH, and there was no acceleration of ice upglacier of Ice Stream B despite reduced effective pressure in this area. Three speedup events occurred in model-CLC, one in 2058, one in 2081 and one in 2098 (Fig. 5g). The largest of these events sped up the ice stream by 47.1 m a^{-1}. None of these ice speedup events registered in the ice speed trend of Ice Stream D. Ice Stream D and Ice Stream E followed similar patterns of slowdown in model-ILC and model-CLC, with ice speed from both models remaining within 10 m a^{-1} of each other in these regions. Like in model-CH, the initial sliding regime of the linear combination friction law follows patterns in the initial hydrology sheet thickness in model-CLC. The sliding regime in model-CLC is in general more Coulomb everywhere than in model-CH, even though the speedup events in model-CLC are of comparable size to those of model-CH. Although the sliding regime of model-CLC is more Coulomb than model-CH, the functional forms of the hydrology-modified Schoof friction law and the linear combination friction law are different, which may explain why the speedup events are of comparable size. As in model-CH, model-CLC has a large negative correlation between the logarithm of the sliding regime and

Downloaded from https://www.cambridge.org/core. 19 Nov 2026 at 14:02:16, subject to the Cambridge Core terms of use.

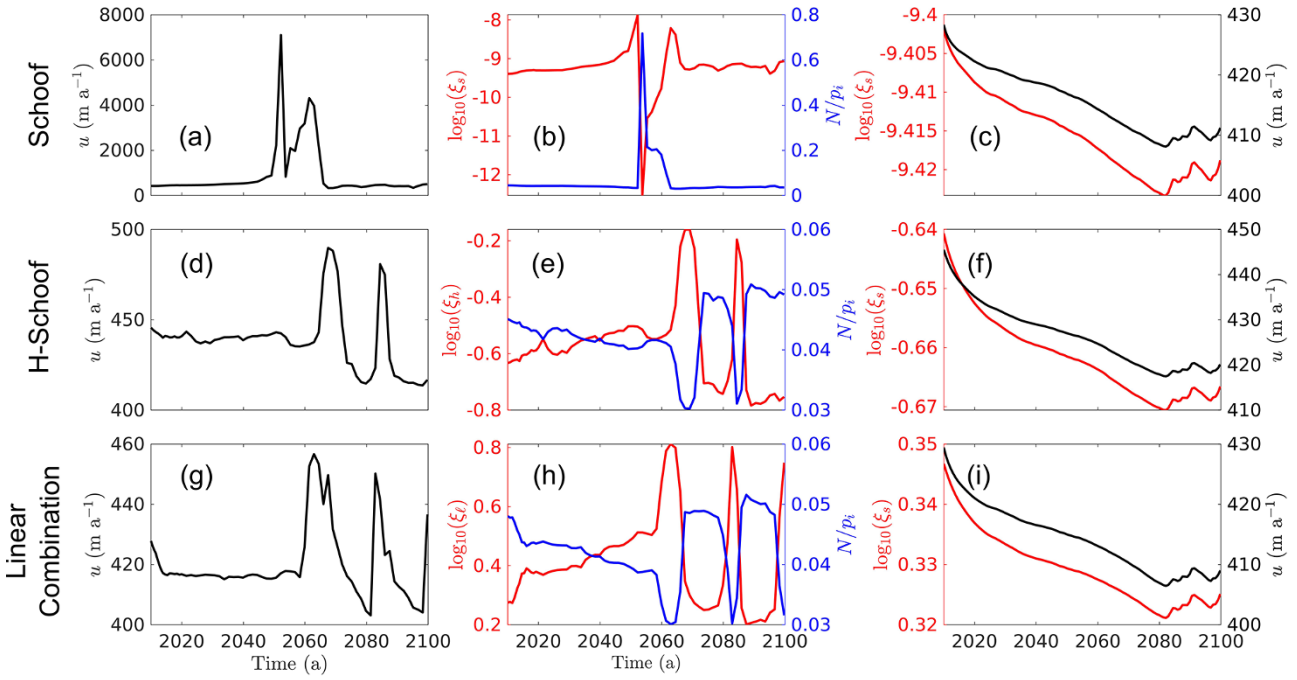


Figure 5. Time series of ice speed, sliding regime (variable controlling the behavior of the friction law) and effective pressure in Ice Stream B for the models with regularized Coulomb friction laws. The left column shows ice speed (m a^{-1}) as a function of time for the coupled model; the middle column shows sliding regime as a function of time in red and the ratio of effective pressure to ice pressure as a function of time in blue for the coupled model; and the right column shows the sliding regime as a function of time in red and ice speed (m a^{-1}) as a function of time in black for the ice flow model. These outputs are shown for the Schoof friction law (a)–(c), the hydrology-modified Schoof friction law (d)–(f) and the linear combination friction law (g)–(i). Please note the different scales used for plotting outputs from the different models.

the ratio of the effective pressure to the ice pressure in Ice Stream B (Fig. 5h, −0.989), and the sliding regime remains nearly constant in model-ILC.

Melt and channelization

Channels formed under the Siple Coast ice streams and in the Byrd trough but had little effect on the dynamics observed in this study. Low hydraulic potential gradients combined with low effective pressure in the Siple Coast resulted in the existence of channels with large area (500 m^2) but limited discharge rate (< 40 m^3 s^{-1}) at the start of the transient simulations. Consequently, little channel evolution was observed. A discussion of channelization from the steady-state GlaDS simulation is given in the Supplementary Material text S3.

Discussion

Here, we analyze how the basal shear stress evolves in relation to changes in basal sliding speed and effective pressure. For an effective pressure dependent sliding/friction law, the basal shear stress evolves as

$$d\tau_b = \frac{\partial \tau_b}{\partial u_b} du_b + \frac{\partial \tau_b}{\partial N} dN, \tag{14}$$

where $d\tau_b$ is an infinitesimal change in the basal shear stress, du_b is an infinitesimal change in the basal ice speed and dN is an infinitesimal change in the effective pressure. For the Budd friction law, the partial derivatives of the basal shear stress are given by

$$\frac{\partial \tau_b}{\partial u_b} = \frac{s\tau_b}{u_b}, \quad \frac{\partial \tau_b}{\partial N} = \frac{r\tau_b}{N}. \tag{15}$$

For the Schoof and hydrology-modified Schoof friction laws, the partials are given by

$$\frac{\partial \tau_b}{\partial u_b} = \frac{m\tau_b}{u_b(1+\xi_i)}, \quad \frac{\partial \tau_b}{\partial N} = \frac{\tau_b \xi_i}{N(1+\xi_i)}, \tag{16}$$

where ξ_i is the sliding regime of the friction law, the parameter ξ_s for the Schoof friction law and ξ_h for the hydrology-modified Schoof friction law, defined in the 'Methods' section. The partial derivatives of the basal shear stress for the linear combination friction law are given by

$$\frac{\partial \tau_b}{\partial u_b} = \frac{C_{\max} N}{u_b} \frac{\xi_\ell}{(1+\xi_\ell)^2} + C_\ell^2 u_b^{m-1} \frac{m + (m-1)\xi_\ell}{(1+\xi_\ell)^2}, \tag{17}$$

$$\frac{\partial \tau_b}{\partial N} = C_{\max} \frac{\xi_\ell (1 - n + \xi_\ell)}{(1+\xi_\ell)^2} + \frac{n C_\ell^2 u_b^m}{N} \frac{\xi_\ell}{(1+\xi_\ell)^2}. \tag{18}$$

For all the regularized Coulomb friction laws (the Schoof friction law, the hydrology-modified Schoof friction law and the linear combination friction law), in the limit that ξ_i goes to 0, we have

$$\left.\frac{\partial \tau_b}{\partial u_b}\right|_{\xi_i \to 0} = \frac{m\tau_b}{u_b}, \quad \left.\frac{\partial \tau_b}{\partial N}\right|_{\xi_i \to 0} = 0, \tag{19}$$

and in the limit that ξ_i goes to ∞ we have

$$\left.\frac{\partial \tau_b}{\partial u_b}\right|_{\xi_i \to \infty} = 0, \quad \left.\frac{\partial \tau_b}{\partial N}\right|_{\xi_i \to \infty} = \frac{\tau_b}{N}. \tag{20}$$

The Budd sliding law

We find that the Budd sliding law is only applicable for running ice flow models in slow moving areas, and we suggest that it is not suitable for two-way coupled modeling. For $r = 1$ and $s = m = 1/n$, as

Downloaded from https://www.cambridge.org/core. 19 Nov 2026 at 14:02:16, subject to the Cambridge Core terms of use.

is commonly chosen for the Budd sliding law, the Budd sliding law responds to changes in basal sliding speed as if the entire domain were in a Weertman sliding regime, and it responds to changes in effective pressure as if the entire domain were in a Coulomb sliding regime. If running an uncoupled or one-way coupled ice flow model, the Budd sliding law would behave exactly like the Weertman sliding law, given the same initial basal shear stress. In regions that should be in a Weertman sliding regime, the Budd sliding law will sufficiently describe the evolution of the basal shear stress. However, when two-way coupled to a subglacial hydrology model, the Budd sliding law will incorrectly describe the evolution of the basal shear stress everywhere, as changes with respect to effective pressure will be incorrect in areas that should be in a Weertman sliding regime, and changes with respect to basal sliding speed will be incorrect in areas that should be in a Coulomb sliding regime. When used for two-way coupled modeling, the Budd sliding law has the ability to produce fast moving ice and low effective pressure in regions that should be in a Weertman sliding regime. This is the consequence of a positive feedback mechanism between effective pressure and ice speed. A decrease (increase) in effective pressure will result in a decrease (increase) in basal shear stress, triggering ice acceleration (deceleration), which will cause dynamic thinning (thickening) of ice, reducing (raising) the hydraulic potential, which will draw more (less) water into the area and lower (raise) the effective pressure. Such a feedback mechanism is possible when trends in ice thickness either match or are overridden by the feedback, and when changes in effective pressure have a larger impact on the basal shear stress than changes in ice speed. That is,

$$\left|\frac{\partial \tau_b}{\partial N} dN\right| > \left|\frac{\partial \tau_b}{\partial u_b} du_b\right|, \tag{21}$$

which, for the Budd sliding law, implies $dN/N > s du_b/(r u_b)$. With $r = 1$ and $s = m = 1/n$, this feedback can occur in relatively slow moving regions ($<100\,\mathrm{m\,a^{-1}}$), as effective pressure is typically between 0 and 20% of ice overburden pressure (92.1% of the grounded domain in model-CH). This feedback was observed upglacier of Ice Stream B in model-CB, showcasing the risks of using the Budd sliding law in two-way coupled modeling. Therefore, the Budd sliding law only agrees with our understanding of sliding over cavities when running ice flow models in slow moving areas with limited cavitation at the glacier bed, and we suggest that it is not suitable for two-way coupled modeling.

The Schoof friction law

We find that the Schoof friction law should only be used for uncoupled or one-way coupled ice flow modeling in slow flowing regions and suggest that it should not be used for two-way coupled modeling on real domains. Under the assumption that the Schoof friction law has a sliding regime that is consistent with the degree of cavitation at the glacier bed, the Schoof friction law will describe the evolution of the basal shear stress in a Weertman sliding regime in a way that is consistent with our understanding of sliding over cavities, in an uncoupled or one-way coupled ice flow model. In a Coulomb sliding regime, where the basal shear stress has a strong effective pressure dependence, two-way coupled modeling is necessary to accurately describe the evolution of the basal shear stress. However, the assumption that the sliding regime is spatially consistent with the degree of cavitation only holds if the ratio of $C_s^2/C_{\max}$ is spatially uniform. Schoof (2005) and Gagliardini and others (2007) modeled ice flow over periodic bedrock protrusions on scales that are much smaller than those of most ice flow modeling studies. Therefore, the resultant regularized Coulomb friction laws were proposed without taking spatially heterogeneous bed conditions (variable C_s and $C_{\max}$) into account. On the small scales considered by Schoof (2005) and Gagliardini and others (2007), and sometimes when modeling synthetic domains, C_s and $C_{\max}$ are spatially uniform and this is not an issue. However, when modeling real domains, $C_{\max}$ is typically chosen to be spatially uniform, while C_s is inverted for, meaning that in practice the sliding regime of the Schoof friction law is not spatially consistent with the degree of cavitation at the glacier bed.

In slow moving regions that should be in a Weertman sliding regime ($\tau_b \approx C_s^2 u_b^m$), the chosen value of $C_{\max}$ will not affect the inversion for C_s. If $C_{\max}$ is chosen to be larger than it should be, the sliding regime will be underestimated, and if $C_{\max}$ is chosen to be smaller than it should be, the sliding regime will be overestimated. However, in both scenarios, the value of C_s determined by the inversion should be accurate, and the sliding regime should in theory remain much $\ll 1$ (Weertman). In fast flowing regions that should be in a Coulomb sliding regime ($\tau_b \approx C_{\max} N$), the basal shear stress is controlled by the value of $C_{\max}$, not C_s. However, the inversion procedure alters the basal shear stress by adjusting C_s, meaning that significant changes in C_s are required to find a basal shear stress that matches simulated and observed ice speed. If $C_{\max}$ is smaller than it should be, then C_s is substantially increased causing a large overestimation in the sliding regime of the friction law. If $C_{\max}$ is larger than it should be, then C_s is substantially reduced, causing a large underestimation in the sliding regime of the friction law. The inversion procedure for C_s is therefore more accurate in regions that should be in a Weertman sliding regime. In model-CS, much of the Siple Coast ice streams were taken to be significantly more Weertman than the surrounding area, and areas that should be in a Weertman sliding regime were marginally overestimated compared to model-CH (Fig. 6).

For the Schoof and hydrology-modified Schoof friction laws, Eqn (21) implies that $dN/N > m du_b/(\xi_i u_b)$. This means that the positive feedback mechanism between effective pressure and ice speed experienced in model-CB is only possible for a sufficiently Coulomb sliding regime when using the Schoof or hydrology-modified Schoof friction laws. In model-CS, the overestimation of the sliding regime in areas that should be Weertman triggered this positive feedback mechanism, resulting in significant acceleration of inland ice. Model-CS illustrates the importance of correctly determining the sliding regime of the Schoof friction law, and the issues that arise from the standard method of determining the basal shear stress with said friction law.

These issues regarding inaccurate estimation of the sliding regime of the Schoof friction law are present not just in two-way coupled models, but in ice flow-only models as well. However, the consequences of such inaccuracies are much more prominent in two-way coupled models. The reasons for this are threefold: (1) the basal shear stress can have at most a cube root ($1/n$) dependence on sliding speed but can have a stronger linear dependence on effective pressure; (2) the magnitude of change in effective pressure is typically comparatively larger than the magnitude of change in the sliding speed ($|dN/N| > |du_b/u_b|$); and (3) in place of the positive feedback mechanism between effective pressure, basal shear stress and ice speed, there is potential for a negative feedback mechanism between sliding speed and basal shear stress since faster sliding increases the basal shear stress but a larger basal shear stress reduces sliding speed. For these reasons, the impacts of the

Downloaded from https://www.cambridge.org/core. 19 Nov 2026 at 14:02:16, subject to the Cambridge Core terms of use.

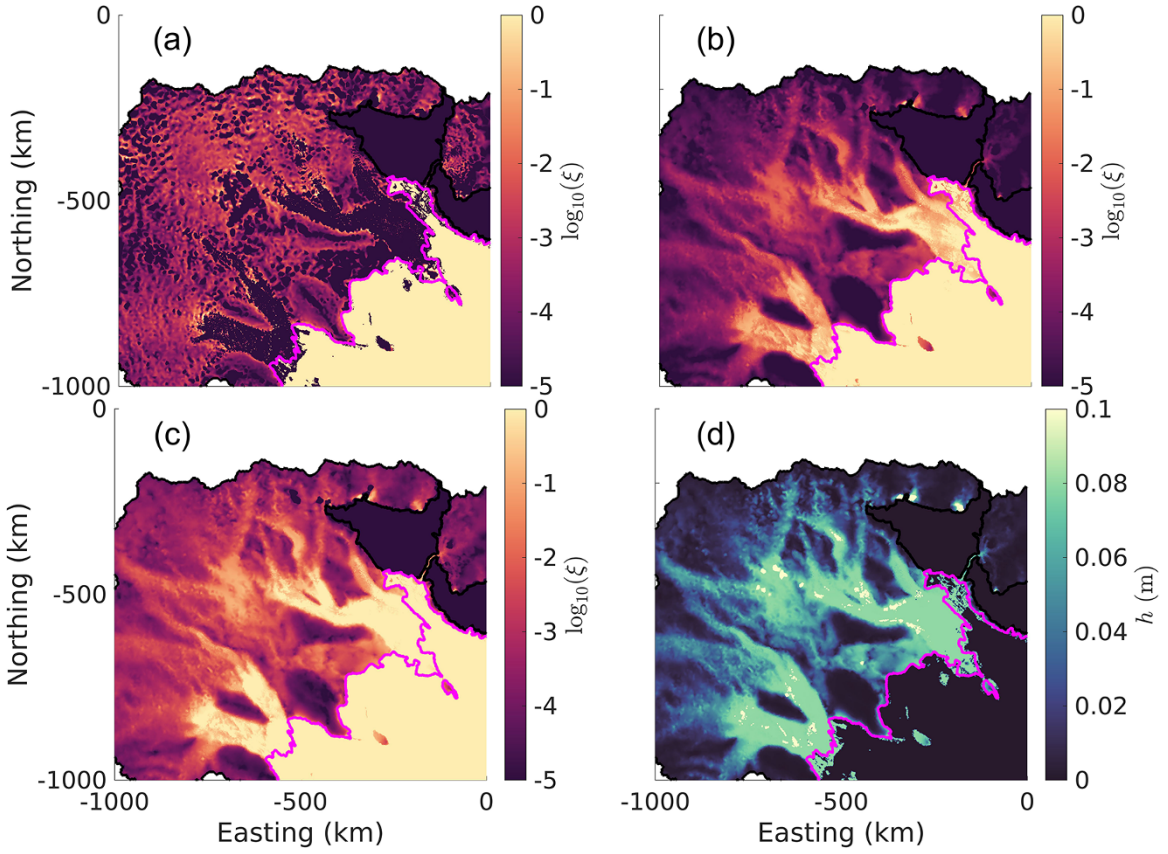


Figure 6. (a) is the initial sliding regime of model-CS; (b) is the initial sliding regime of model-CH; (c) is the initial sliding regime of model-CLC; and (d) is the initial hydrology sheet thickness (m) of model-CH. The pink lines represent the grounding line at the start of the simulations and the black lines represent the domain boundary.

incorrect sliding regime of the Schoof friction law are less obvious in ice flow-only models.

Given the impact of the inversion procedure for C_s on the sliding regime of the Schoof friction law, we suggest that the Schoof friction law should only be used for uncoupled or one-way coupled ice flow modeling in slow flowing regions with low cavitation, and it should not be used for two-way coupled modeling on real domains. This is the same conclusion we arrived at for the Budd friction law, though for different reasons. When using a Schoof friction law in an uncoupled or one-way coupled ice flow model, the basal shear stress still responds to changes in basal sliding speed based on the sliding regime of the friction law; however, the sliding regime of the friction law is not spatially consistent with the degree of cavitation at the glacier bed. In contrast, the Budd friction law responds to changes in the basal sliding speed as if the entire domain were in a completely Weertman sliding regime. The Schoof friction law may therefore be more desirable than the Budd friction law if running an uncoupled or one-way coupled ice flow model in a slow flowing region.

New friction laws

We find that the hydrology-modified Schoof and linear combination friction laws are suitable for modeling slow flowing regions with a one-way coupled or uncoupled model and can be used to model any grounded region of a glacier with a two-way coupled model. Unlike the Schoof friction law, the hydrology-modified Schoof friction law ensures that the sliding regime of the friction law is spatially consistent with the degree of cavitation at the glacier bed. Therefore, with an appropriate effective pressure input, the hydrology-modified Schoof friction law will describe the evolution of the basal shear stress in a Weertman sliding regime, in a way that is consistent with our understanding of sliding over cavities, even in a one-way coupled model. In a two-way coupled model, the hydrology-modified Schoof friction law will describe the evolution of the basal shear stress in a way that is consistent with our understanding of sliding over cavities throughout the model domain. However, by fixing the ratio of $C_h^2/C_{\max} = \zeta$, the inversion for C_h also determines Iken's bound. That is, C_h and $C_{\max}$ cannot be chosen independently. C_h is dependent on the ratio of bedrock bump size to spacing (Weertman, 1957), and $C_{\max}$ is the maximum angle on the stoss face of bedrock bumps (Iken, 1981; Schoof, 2005). These two ideas are physically independent of each other, yet, in the hydrology-modified Schoof friction law, Iken's bound is determined by the inversion for C_h. In areas with low cavitation, the inversion procedure chooses C_h such that $\tau_b \approx C_h^2 u_b^m$, and in areas with high cavitation, the inversion procedure chooses C_h such that $\tau_b \approx C_h^2 N/\zeta$. Therefore, the value of C_h determined by the inversion procedure only remains accurate during transient model simulations while the current sliding regime remains similar to the initial sliding regime that the inversion was performed on. That is, large changes in the degree of cavitation at the glacier bed (switches between Weertman and Coulomb sliding) may lead to an evolution of the basal shear stress that is not consistent with our understanding of sliding over cavities. The Kamb Ice Stream did not reactivate in the timeframe of any of our models, but if

Downloaded from https://www.cambridge.org/core. 19 Nov 2026 at 14:02:16, subject to the Cambridge Core terms of use.

it did, the hydrology-modified Schoof friction law may be insufficient to accurately describe such a reactivation where there would be a transition from Weertman to Coulomb sliding.

The different functional form between the linear combination friction law and the Schoof/hydrology-modified Schoof friction laws means that areas with sliding regimes between Weertman and Coulomb are dealt with differently. While we know how friction laws should behave in the limit of Weertman and Coulomb sliding, it is unclear how to deal with these areas in between, and future work on the development of basal friction laws should consider these regions. The primary benefit of the linear combination friction law is having the ability to choose Weertman and Coulomb friction parameters while having a sliding regime that is spatially consistent with the degree of cavitation at the glacier bed. However, the value of $C_{\max}$ was chosen to be spatially uniform in the linear combination friction law, as there is no good alternative to choosing both C_ℓ and $C_{\max}$ at the moment. Future work should focus on a methodology to constrain both $C_{\max}$ and C_ℓ simultaneously. Such a methodology would likely need to go beyond a snapshot inversion, which for strong Weertman and Coulomb sliding regimes will only be able to accurately constrain C_ℓ or $C_{\max}$ respectively. Likely, a relationship between Weertman and Coulomb friction parameters must be identified (if one exists) through studying areas with temporally variable bed conditions, such as surging glaciers, or glaciers with seasonal velocity patterns. If such a relationship can be identified, then an inversion could be used to constrain both parameters simultaneously. Alternatively, these parameters could be constrained through other means, such as using geologic information.

Although the linear combination friction law offers desirable properties that the Budd, Schoof and hydrology-modified Schoof friction laws lack, it is not derived from first principals and is not consistent with the criteria outlined by Gagliardini and others (2007) that a friction law should follow. In particular, Iken's bound is not strictly enforced. When $\xi_\ell > \alpha(C_{\max}/C_\ell^2)^n$, then $\tau_b > C_{\max}N$. For large ξ_ℓ, we can Taylor expand Eqn (12) and find

$$\tau_b \approx C_{\max}N + \xi_\ell^{-1+1/n}\frac{C_\ell^2}{\alpha^{1/n}C_{\max}} - \xi_\ell^{-1}. \tag{22}$$

So, for sufficiently large α, and large ξ_ℓ where the bound is most important, the bound will very approximately hold. Therefore, the relationship between the basal shear stress and effective pressure not strictly obeying Iken's bound has the largest potential impact on areas intermediate to Weertman and Coulomb sliding, which have not been a focus in the development of past friction laws. The new regularized Coulomb friction laws analyzed in this study balance desirable properties from theoretical analyses of basal sliding with the practical necessities required to model real domains. Additional investigation into a more appropriate functional form of the friction law that can encompass all of these properties is necessary.

The hydrology-modified Schoof friction law achieves a unified description of subglacial conditions between the friction law and subglacial hydrology model through constricting parameter values of the friction law. An alternative approach is to keep the friction law unaltered and constrict the parameter values of the subglacial hydrology model. This is similar to the approach of Gilbert and others (2022) and Togaibekov and others (2024), who reformulated the friction law and subglacial hydrology model in terms of a dimensionless 'cavitation state' variable. The cavitation state was defined so that the friction law would be unaltered, and the sheet conductivity and sheet thickness were reformulated in terms of a power law dependence on the cavitation state. The cavitation state evolved due to opening from sliding and closing from ice creep, written in terms of the friction law parameters. In this study, we have instead focused on the development of friction laws that are consistent with subglacial hydrology models. However, it is really a consistent description of basal conditions between the friction law and subglacial hydrology model that is important, and this can be achieved through alternative means, as done in Gilbert and others (2022), Togaibekov and others (2024). In the context of our study, the Schoof friction law could be made to have a sliding regime that is spatially consistent with the degree of cavitation through varying ℓ_r so that it is proportional to $C_{\max}/(C_s^2\tilde{A})$. However, this would create a much more difficult inversion problem to solve when modeling real domains, as varying ℓ_r will vary the effective pressure, which the basal shear stress is dependent on. Furthermore, there is no inherent advantage to choosing a value of C_s over choosing a value of ℓ_r (as done in this study), as there are, in general, limited geophysical observations of basal conditions to constrain either parameter.

The assumption of steady-state hydrology

The hydrology-modified Schoof friction law and the linear combination friction law assume that the hydrology sheet thickness is in steady state, so that u_b/N^n is completely determined by h. This is in general a good assumption, as an order of magnitude approximation of the hydrology sheet opening rate gives $\omega_s \approx 10^{-8}\,\mathrm{m\,s^{-1}}$ ($u_b \approx 10\,\mathrm{m\,a^{-1}}$, $h_r - h \approx 0.1\,\mathrm{m}$, $\ell_r \approx 1\,\mathrm{m}$) for a Weertman sliding regime, and for a Coulomb sliding regime $\omega_s \approx 10^{-8}\,\mathrm{m\,s^{-1}}$ ($u_b \approx 1000\,\mathrm{m\,a^{-1}}$, $h_r - h \approx 0.001\,\mathrm{m}$). $\frac{\partial h}{\partial t}$ typically changes on the order of $10^{-12}\,\mathrm{m\,s^{-1}}$ meaning that ω_s and ν_s are the dominant terms in Eqn (4). Still, in regions where there is fast evolution of the hydrology sheet thickness ($\frac{\partial h}{\partial t}$ balances the opening or closing term in Eqn 4), Eqn (11) will no longer be applicable. On a related note, the friction law criteria proposed by Gagliardini and others (2007) is based on a steady-state assumption, and the regularized Coulomb friction laws developed based on this work are also likely not applicable in these regions.

Effective pressure dependent friction laws calculate the basal friction of a steady-state hydrology system characterized by the effective pressure. Alternatively, Thøgersen and others (2019) and Gilbert and others (2022) proposed regularized Coulomb friction laws that calculate the basal friction of a steady-state hydrology system characterized by subglacial cavitation. Similarly, we can use Eqn (11) to reformulate the hydrology-modified Schoof and linear combination friction laws in terms of h. For the hydrology-modified Schoof friction law, we have

$$\tau_b = \frac{C_h^2\,|\overrightarrow{u_b}|^{m-1}}{(1+\zeta^{1/m}\tilde{A}\ell_r h/(h_r-h))^m}\overrightarrow{u_b}, \tag{23}$$

and for the linear combination friction law we have

$$\tau_b = C_{\max}N_h\,|\overrightarrow{u_b}|^{-1}\,\overrightarrow{u_b}\left(\frac{\xi_\ell}{1+\xi_\ell}\right) + C_\ell^2\,|\overrightarrow{u_b}|^{m-1}\,\overrightarrow{u_b}\left(\frac{1}{1+\xi_\ell}\right), \tag{24}$$

$$\xi_\ell = \alpha\tilde{A}\ell_r\frac{h}{h_r-h}, \quad N_h = \left(\frac{u_b(h_r-h)}{\tilde{A}\ell_r h}\right)^m. \tag{25}$$

We refer to Eqns (23) and (24) as the 'cavity' formulation of the hydrology-modified Schoof and linear combination friction laws, and we refer to the original Eqns (9) and (12) as the 'pressure'

Downloaded from https://www.cambridge.org/core. 19 Nov 2026 at 14:02:16, subject to the Cambridge Core terms of use.

formulation. If we define h_N to be the steady-state sheet thickness for a given effective pressure (calculated from rearranging Eqn 11), then the pressure formulation of the hydrology-modified Schoof friction law and the linear combination friction law can be written in the form of Eqns (23) and (24), respectively, with h replaced by h_N, and N_h replaced with N for the linear combination friction law. Furthermore, for an evolving hydrology sheet, h is transitioning toward h_N. So, the cavity formulation can be thought of as describing basal friction of the past system, and the pressure formulation can be thought of as describing basal friction of where the system is headed. Therefore, basal friction should be intermediate to that predicted from the cavity formulation and that predicted from the pressure formulation. This can be described using Eqns (23) and (24) with $\tilde{h} = \lambda h + (1-\lambda)h_N$ in place of h, where $\lambda \in [0,1]$ is a parameter that controls the importance of where the system was vs where the system is headed. For the hydrology-modified Schoof friction law, this gives

$$\tau_b = \frac{C_h^2 \left|\overrightarrow{u_b}\right|^{m-1}}{\left(1+\zeta^{1/m}\tilde{A}\ell_r\tilde{h}/(h_r-\tilde{h})\right)^m}\overrightarrow{u_b}, \tag{26}$$

and for the linear combination friction law this gives

$$\tau_b = C_{\max}\tilde{N}\left|\overrightarrow{u_b}\right|^{-1}\overrightarrow{u_b}\left(\frac{\xi_\ell}{1+\xi_\ell}\right) + C_\ell^2\left|\overrightarrow{u_b}\right|^{m-1}\overrightarrow{u_b}\left(\frac{1}{1+\xi_\ell}\right), \tag{27}$$

$$\xi_\ell = \alpha\tilde{A}\ell_r\frac{\tilde{h}}{h_r-\tilde{h}}, \quad \tilde{N} = \left(\frac{u_b(h_r-\tilde{h})}{\tilde{A}\ell_r\tilde{h}}\right)^m. \tag{28}$$

If $\lambda = 0$, we recover the pressure formulation, and if $\lambda = 1$, we recover the cavity formulation. Equations (26) and (27) also provide a sliding regime that is intermediate to that of the cavity formulation and the pressure formulation, which is also likely more applicable in regions where there is a rapidly evolving hydrology sheet.

Uncoupled ice flow models

In ice flow modeling studies, the effective pressure is often not determined by running a subglacial hydrology model, with an effective pressure parameterization being used in the basal friction law instead. These parameterizations are often poor estimators of the effective pressure and are in some cases nonphysical (McArthur and others, 2023). The standard parameterization used is actually the overburden hydraulic potential with the density of freshwater replaced with the density of salt water, $N = \phi_0 = \rho_i g H + \rho_{sw} g B$. This parameterization assumes perfect hydraulic connectivity to the ocean (subglacial water pressure is equal to hydrostatic pressure at the grounding line) but leads to unrealistically large values of effective pressure away from the grounding line. In fact, when the bed elevation is above sea level, this parameterization implies negative subglacial water pressure, which is not physical. This large overestimation of effective pressure will lead to a large underestimation in the sliding regime of the friction law. McArthur and others (2023) proposed an empirical parameterization of the effective pressure, motivated from subglacial hydrology modeling of Denman Glacier, East Antarctica. This parameterization is based on the idea that the flotation fraction (fraction of subglacial water pressure relative to ice overburden pressure) decreases as the ice thickness increases, an idea that does not work well for topographically unconstrained ice streams such as those in the Siple Coast. Still, this empirical parameterization ensures the effective pressure does not reach nonphysically large values (larger than ice overburden pressure) and resulting significant underestimations of the sliding regime of the friction law. Two-way coupled models are computationally more expensive than uncoupled ice flow models and have added modeling complexities (such as complicated initialization procedures) that will make two-way coupled modeling undesirable in some cases. In these situations, improved effective pressure parameterizations are necessary to describe basal conditions in fast flowing Coulomb sliding regimes, which are often of interest.

The impact of depth averaging on basal friction

In this study, we used a 2-D ice flow model, with depth-averaged ice velocity. Therefore, the basal ice speed is likely overestimated, particularly in areas where there should be Weertman sliding, and ice motion is primarily a result of internal deformation. An overestimation of the ice velocity implies there is an underestimation in the basal friction coefficient, so that the same basal shear stress is achieved. In a strong Weertman sliding regime, where an increase in ice surface speed may not reflect the onset of basal sliding, there should be an overestimation of basal friction in our models. However, in a transition from Weertman to Coulomb sliding, where Iken's bound becomes the relevant friction parameter, friction is likely underestimated in the hydrology-modified Schoof friction law, where $C_{\max} = C_h^2/\zeta$. In the Schoof and linear combination friction laws, this should be less of an issue as Iken's bound is chosen independently of the Weertman friction parameter. Due to the dependence of the friction law on basal ice motion, a 3-D ice flow model is desirable for modeling slow moving ice in a Weertman sliding regime. However, even a 2-D model with a vertically heterogeneous ice velocity such as the MOno-Layer Higher-Order (Dias dos Santos and others, 2022) model is preferable over the SSA. In a Coulomb sliding regime, a 2-D ice flow model with the linear combination friction law should more appropriately describe the evolution of the basal shear stress compared to a Weertman sliding regime.

Conclusions

In this study, we investigated the impact of the friction law on ice flow modeling using one-way and two-way coupled ice flow/subglacial hydrology models in the Siple Coast as a case study. Additionally, we presented two new regularized Coulomb friction laws, developed specifically for two-way coupled modeling.

It is clear from the results of this study that the present implementation of basal friction in ice flow modeling leaves room for improvement. We have found that one-way coupled or uncoupled ice flow models can sufficiently describe ice motion in a Weertman sliding regime. However, fast moving, highly cavitated areas that are in a Coulomb sliding regime require the use of two-way coupled modeling where the evolution of the basal shear stress is dominated by changes in effective pressure to capture the physical processes present in those regions. The Budd sliding law and the Schoof friction law, which are commonly used in ice flow modeling studies, were found to be unsuitable for two-way coupled modeling. When using the Budd sliding law, the basal shear stress responded to changes in ice speed as if the entire domain were in a Weertman sliding regime and responded to changes in effective pressure as if the entire domain were in a Coulomb sliding regime. The latter resulted in a positive feedback mechanism that significantly increased the speed of inland ice while simultaneously flooding

Downloaded from https://www.cambridge.org/core. 19 Nov 2026 at 14:02:16, subject to the Cambridge Core terms of use.

the subglacial hydrologic system. The sliding regime of regularized Coulomb friction laws was found to be an important factor, which controls the evolution of the basal shear stress. The Schoof friction law has a sliding regime that is not dependent on the degree of cavitation at the glacier bed in a spatially consistent fashion, which led to the same feedback mechanism experienced with the Budd friction law.

In light of the limitations of the Budd and Schoof friction laws, we proposed and tested two additional regularized Coulomb friction laws that have a sliding regime that is spatially consistent with the degree of cavitation at the glacier bed. The first is a version of the Schoof friction law that we modified so that $C_s^2/C_{\max}$ is spatially uniform, called the 'hydrology-modified Schoof friction law', and the second is a linear combination of Weertman and Coulomb sliding terms with coefficients that sum to one and are dependent on the sliding regime of the friction law, called the 'linear combination friction law'. These friction laws did not lead to nonphysically large changes in ice motion despite a similar reduction of effective pressure upglacier of Ice Stream B, albeit on a much smaller scale. Furthermore, the linear combination friction law is able to choose Coulomb and Weertman friction parameters (C_ℓ and $C_{\max}$), while simultaneously having a sliding regime that is spatially consistent with the degree of cavitation at the glacier bed. However, it still requires the modeler to choose the value of Iken's bound, which introduces additional uncertainties to the model.

We have identified the importance of including evolving effective pressure in basal friction parameterizations, having a sliding regime that is spatially consistent with the degree of cavitation at the glacier bed and having the ability to choose both Coulomb and Weertman friction parameters. However, additional work is necessary to describe the evolution of basal friction in ice flow modeling in a way that is consistent with our understanding of sliding over cavities. In particular, a procedure must be developed to choose Weertman and Coulomb friction parameters simultaneously, the ideal functional form of the friction law must be investigated, and improved effective pressure parameterizations must be developed and implemented in uncoupled ice flow models.

Supplementary material. The supplementary material for this article can be found at https://doi.org/10.1017/jog.2026.10216.

Data availability statement. We use version 4.24 of the open-source ISSM software; ISSM is available for download from https://github.com/ISSMteam/ISSM. The datasets used in the initialization procedure are available at the references cited in the main text of this manuscript. Model outputs and scripts for running the models can be found at McArthur and others (2026b).

Acknowledgements. K.R.K.M. was supported by the Natural Sciences and Engineering Research Council of Canada (NSERC), Canada Graduate Scholarship and the Ontario Graduate Scholarship. C.F.D. was supported by NSERC (NSERC RGPIN-03761-2017 and RGPIN-2025-03982) and by the Canada Research Chairs Program. S.E. was supported by NSERC (NSERC RGPIN-03761-2017). The authors would like to thank the Digital Research Alliance of Canada for access to supercomputing resources. The authors would like to thank the scientific editor Alan Rempel and three anonymous reviewers for their suggestions to improve this manuscript.

References

Adusumilli S, Fricker HA, Medley B, Padman L and Siegfried M (2020) Interannual variations in meltwater input to the Southern Ocean from Antarctic ice shelves. *Nature Geoscience* **13**(9), 616–620. doi: 10.1038/s41561-020-0616-z.

Beem LH, Tulaczyk SM, King MA, Bougamont M, Fricker HA and Christoffersen P (2014) Variable deceleration of Whillans Ice Stream, West Antarctica. *Journal of Geophysical Research: Earth Surface* **119**(2), 212–224. doi: 10.1002/2013JF002958.

Blankenship DD, Bentley CR, Rooney ST and Alley RB (1986) Seismic measurements reveal a saturated porous layer beneath an active Antarctic ice stream. *Nature* **322**(6074), 54–57. doi: 10.1038/322054a0.

Bougamont M, Christoffersen P, Price SF, Fricker HA, Tulaczyk S and Carter SP (2015) Reactivation of Kamb Ice Stream tributaries triggers century-scale reorganization of Siple Coast ice flow in West Antarctica. *Geophysical Research Letters* **42**(20), 8471–8480. doi: 10.1002/2015GL065782.

Bougamont M, Price S, Christoffersen P and Payne AJ (2011) Dynamic patterns of ice stream flow in a 3-D higher-order ice sheet model with plastic bed and simplified hydrology. *Journal of Geophysical Research: Earth Surface* **116**(F4) doi: 10.1029/2011JF002025.

Brondex J, Gillet-Chaulet F and Gagliardini O (2019) Sensitivity of centennial mass loss projections of the Amundsen basin to the friction law. *The Cryosphere* **13**(1), 177–195.

Budd WF, Keage PL and Blundy NA (1979) Empirical studies of ice sliding. *The Journal of Glaciology* **23**(89), 157–170. doi: 10.3189/S0022143000029804.

Catania G, Hulbe C, Conway H, Scambos T and Raymond C (2012) Variability in the mass flux of the Ross ice streams, West Antarctica, over the last millennium. *The Journal of Glaciology* **58**(210), 741–752 10.3189/2012JoG11J219

Cook SJ, Christoffersen P and Todd J (2022) A fully-coupled 3D model of a large Greenlandic outlet glacier with evolving subglacial hydrology, frontal plume melting and calving. *The Journal of Glaciology* **68**(269), 486–502. doi: 10.1017/jog.2021.109.

Covington MD, Gulley JD, Trunz C, Mejia J and Gadd W (2020) Moulin volumes regulate subglacial water pressure on the Greenland Ice Sheet. *Geophysical Research Letters* **47**(20), doi: 10.1029/2020GL088901.

Cuffey K and Paterson W (2010) *The Physics of Glaciers*. Elsevier Science, ISBN 9780123694614.

Dias dos Santos T, Morlighem M and Brinkerhoff D (2022) A new vertically integrated MOno-Layer Higher-Order-(MOLHO) ice flow model. *The Cryosphere* **16**(1), 179–195. doi: 10.5194/tc-16-179-2022.

Dow C, McCormack F, Young D, Greenbaum J, Roberts J and Blankenship D (2020) Totten Glacier subglacial hydrology determined from geophysics and modeling. *Earth and Planetary Science Letters* **531**, doi: 10.1016/j.jpgl.2019.115961.

Dow CF, Ross N, Jeofry H, Siu K and Siegert MJ (2022) Antarctic basal environment shaped by high-pressure flow through a subglacial river system. *Nature Geoscience* **15**(11), 892–898. doi: 10.1038/s41561-022-01059-1.

Ehrenfeucht S, Dow C, McArthur K, Morlighem M and McCormack FS (2025) Antarctic wide subglacial hydrology modeling. *Geophysical Research Letters* **52**(1), doi: 10.1029/2024GL111386.

Ehrenfeucht S, Morlighem M, Rignot E, Dow CF and Mouginot J (2023) Seasonal acceleration of Petermann Glacier, Greenland, from changes in subglacial hydrology. *Geophysical Research Letters* **50**(1), doi: 10.1029/2022GL098009.

Engelhardt H, Humphrey N, Kamb B and Fahnestock M (1990) Physical conditions at the base of a fast moving Antarctic ice stream. *Science (American Association for the Advancement of Science)* **248**(4951), 57–59. doi: 10.1126/science.248.4951.57.

Engelhardt H and Kamb B (1998) Basal sliding of Ice Stream B, West Antarctica. *Journal of Glaciology* **44**(147), 223–230. doi: 10.3189/S0022143000002562.

Flowers GE and Clarke GKC (2002a) A multicomponent coupled model of glacier hydrology 1. Theory and synthetic examples. *Journal of Geophysical Research-Solid Earth* **107**(B11), ECV 9–1–ECV 9–17. doi: 10.1029/2001JB001122.

Flowers GE and Clarke GKC (2002b) A multicomponent coupled model of glacier hydrology 2. Application to Trapridge Glacier, Yukon, Canada. *Journal of Geophysical Research-Solid Earth* **107**(B11), ECV 10–1–ECV 10–16 doi: 10.1029/2001JB001124.

Fowler A (2010) Weertman, Lliboutry and the development of sliding theory. *Journal of Glaciology* **56**(200), 965–972. doi: 10.3189/002214311796406112.

Downloaded from https://www.cambridge.org/core. 19 Nov 2026 at 14:02:16, subject to the Cambridge Core terms of use.

Gagliardini O, Cohen D, Råback P and Zwinger T (2007) Finite-element modeling of subglacial cavities and related friction law. *Journal of Geophysical Research* **112**(F2), F02027. doi: 10.1029/2006JF000576.

Gagliardini O and Werder MA (2018) Influence of increasing surface melt over decadal timescales on land-terminating Greenland-type outlet glaciers. *Journal of Glaciology* **64**(247), 700–710. doi: 10.1017/jog.2018.59.

Gilbert A, Gimbert F, Thøgersen K, Schuler TV and Kääb A (2022) A consistent framework for coupling basal friction with subglacial hydrology on hard-bedded glaciers. *Geophysical Research Letters* **49**(13), e2021GL097507. doi: 10.1029/2021GL097507.

Glen JW and Perutz MF (1955) The creep of polycrystalline ice. *Proc. of the Royal Soc. of London. Series A. Math. and Phys. Sciences* **228**(1175), 519–538. doi: 10.1098/rspa.1955.0066.

Hewitt I (2013) Seasonal changes in ice sheet motion due to melt water lubrication. *Earth and Planetary Science Letters* **371–372**, 16–25. doi: 10.1016/j.jpgl.2013.04.022.

Hoffman M and Price S (2014) Feedbacks between coupled subglacial hydrology and glacier dynamics. *Journal of Geophysical Research-Earth Surface* **119**(3), 414–436. doi: 10.1002/2013JF002943.

Iken A (1981) The effect of the subglacial water pressure on the sliding velocity of a glacier in an idealized numerical model. *Journal of Glaciology* **27**(97), 407–421. doi: 10.3189/S0022143000011448.

Iverson NR, Hooyer TS and Baker RW (1998) Ring-shear studies of till deformation: Coulomb-plastic behavior and distributed strain in glacier beds. *Journal of Glaciology* **44**(148), 634–642. doi: 10.3189/S0022143000002136.

Joughin I, Smith BE and Schoof CG (2019) Regularized coulomb friction laws for ice sheet sliding: Application to Pine Island Glacier, Antarctica. *Geophysical Research Letters* **46**(9), 4764–4771. doi: 10.1029/2019GL082526.

Kamb B (1987) Glacier surge mechanism based on linked cavity configuration of the basal water conduit system. *Journal of Geophysical Research-Solid Earth* **92**(B9), 9083–9100. doi: 10.1029/JB092iB09p09083.

Kittel C and 10 others (2021) The Cryosphere: MAR and ESMs data. doi: 10.5281/zenodo.4459259.

Kittel C and 10 others (2021) Diverging future surface mass balance between the Antarctic ice shelves and grounded ice sheet. *The Cryosphere* **15**(3), 1215–1236. doi: 10.5194/tc-15-1215-2021.

Larour E, Seroussi H, Morlighem M and Rignot E (2012) Continental scale, high order, high spatial resolution, ice sheet modeling using the Ice Sheet System Model (ISSM). *Journal of Geophysical Research-Earth Surface* **117**(F1), F01022. doi: 10.1029/2011JF002140.

Lliboutry L (1959) Une théorie du frottement du glacier sur son lit. *Annales de Géophysique* **15**, 250.

Lliboutry L (1968) General theory of subglacial cavitation and sliding of temperate glaciers. *Journal of Glaciology* **7**(49), 21–58. doi: 10.3189/S0022143000020396.

Lu G and Kingslake J (2024) Two-way coupling between ice flow and channelized subglacial drainage enhances modeled marine-ice-sheet retreat. *The Cryosphere* **18**(11), 5301–5321. doi: 10.5194/tc-18-5301-2024.

MacAyeal DR (1989) Large-scale ice flow over a viscous basal sediment: Theory and application to ice stream B, Antarctica. *Journal of Geophysical Research* **94**(B4), 4071–4087. doi: 10.1029/JB094iB04p04071.

MacAyeal DR (1993) A tutorial on the use of control methods in ice-sheet modeling. *Journal of Glaciology* **39**(131), 91–98. doi: 10.3189/S0022143000015744.

McArthur K, Dow C and Ehrenfeucht S (2026a) Exploring Antarctic feedback mechanisms using two-way coupled subglacial hydrology and ice flow modeling in the Siple Coast. *Geophysical Research Letters* **53**(15), e2025GL121190. doi: 10.1029/2025GL121190.

McArthur K, Dow C and Ehrenfeucht S (2026b) The impact of the friction law on coupled subglacial hydrology and ice flow modeling. doi: 10.5281/zenodo.19462449.

McArthur K, McCormack FS and Dow CF (2023) Basal conditions of Denman Glacier from glacier hydrology and ice dynamics modeling. *The Cryosphere* **17**(11), 4705–4727. doi: 10.5194/tc-17-4705-2023.

Meyer CR, Warburton KLP, Sommers AN and Minchew BM (2026) A model of water extraction from the subglacial hydrologic system under idealized conditions. *The Cryosphere* **20**(5), 2659–2680. doi: 10.5194/tc-20-2659-2026.

Morlighem M and 10 others (2020) Deep glacial troughs and stabilizing ridges unveiled beneath the margins of the Antarctic ice sheet. *Nature Geoscience* **13**, 132–137. doi: 10.1038/s41561-019-0510-8.

Morlighem M, Seroussi H, Larour E and Rignot E (2013) Inversion of basal friction in Antarctica using exact and incomplete adjoints of a higher-order model. *Journal of Geophysical Research-Earth Surface* **118**(3), 1746–1753. doi: 10.1002/jgrf.20125.

Mouginot J, Rignot E, Scheuchl B and Millan R (2017) Comprehensive annual ice sheet velocity mapping using Landsat-8, Sentinel-1, and RADARSAT-2 data. *Remote Sensing* **9**(4), 364. doi: 10.3390/rs9040364.

Mouginot J, Scheuchl B and Rignot E (2012) Mapping of ice motion in Antarctica using Synthetic-Aperture Radar data. *Remote Sensing* **4**(9), 2753–2767. doi: 10.3390/rs4092753.

Pelle T, Greenbaum JS, Ehrenfeucht S, Dow CF and McCormack FS (2024) Subglacial discharge accelerates dynamic retreat of aurora subglacial basin outlet glaciers, East Antarctica, over the 21st century. *Journal of Geophysical Research-Earth Surface* **129**(7), doi: 10.1029/2023JF007513.

Röthlisberger H (1972) Water pressure in intra- and subglacial channels. *Journal of Glaciology* **11**(62), 177–203. doi: 10.3189/S0022143000022188.

Rignot E, Mouginot J and Scheuchl B (2011) Ice flow of the Antarctic ice sheet. *Science* **333**(6048), 1427–1430. doi: 10.1126/science.1208336.

Rignot E, Mouginot J and Scheuchl B (2017) MEaSUREs InSAR-Based Antarctica ice velocity map, version 2 [data set]. Boulder, Colorado USA. NASA National Snow and Ice Data Center Distributed Active Archive Center. doi: 10.5067/D7GK8F5J8M8R.

Schoof C (2005) The effect of cavitation on glacier sliding. *Proc. of the Royal Soc. A, Math. Phys. and Eng. Sciences* **461**, 609–627. doi: 10.1098/rspa.2004.1350.

Seroussi H and 38 others (2019) initMIP-Antarctica: An ice sheet model initialization experiment of ISMIP6. *The Cryosphere* **13**(5), 1441–1471. doi: 10.5194/tc-13-1441-2019.

Seroussi H and 46 others (2020) ISMIP6 Antarctica: A multi-model ensemble of the Antarctic ice sheet evolution over the 21st century. *The Cryosphere* **14**(9), 3033–3070. doi: 10.5194/tc-14-3033-2020.

Sommers A, Rajaram H and Morlighem M (2018) SHAKTI: Subglacial Hydrology and Kinetic, Transient Interactions v1.0. *Geoscientific Model Development* **11**(7), 2955–2974. doi: 10.5194/gmd-11-2955-2018.

Sommers AN and 7 others (2024) Velocity of Greenland's Helheim Glacier controlled both by terminus effects and subglacial hydrology with distinct realms of influence. *Geophysical Research Letters* **51**(15), e2024GL109168. doi: 10.1029/2024gl109168.

Stål T, Reading AM, Halpin JA and Whittaker J (2020) *Antarctic Geothermal Heat Flow model: Aq1*. PANGAEA. doi: 10.1594/PANGAEA.924857.

Stål T, Reading AM, Halpin JA and Whittaker JM (2021) Antarctic Geothermal Heat Flow Model: Aq1. *Geochemistry, Geophysics, Geosystems: G3* **22**(2), e2020GC009428. doi: 10.1029/2020GC009428.

Thøgersen K, Schuler T, Gilbert A and Malthe-Sørenssen A (2019) Rate-and-state friction explains glacier surge propagation. *Nature Communications* **10**(1), 2823–8. doi: 10.1038/s41467-019-10506-4.

Togaibekov A, Gimbert F, Gilbert A and Walpersdorf A (2024) Observing and modeling short-term changes in basal friction during rain-induced speed-ups on an alpine glacier. *Geophysical Research Letters* **51**(14), e2023GL107999. doi: 10.1029/2023GL107999.

Tulaczyk S, Kamb WB and Engelhardt HF (2000) Basal mechanics of Ice Stream B, West Antarctica: 2. Undrained plastic bed model. *Journal of Geophysical Research: Solid Earth* **105**(B1), 483–494. doi: 10.1029/1999JB900328.

van Wessem JM, van de Berg WJ and van den Broeke MR. (2023). Data set: Monthly averaged RACMO2.3p2 variables. Antarctica. doi: 10.5281/zenodo.7760491.

Walder JS and Fowler A (1994) Channelized subglacial drainage over a deformable bed. *Journal of Glaciology* **40**(134), 3–15. doi: 10.3189/S0022143000003750.

Downloaded from https://www.cambridge.org/core. 19 Nov 2026 at 14:02:16, subject to the Cambridge Core terms of use.

Walder JS (1986) Hydraulics of subglacial cavities. *Journal of Glaciology* **32**(112), 439–445. doi: 10.3189/S0022143000012156.

Weertman J (1957) On the sliding of glaciers. *Journal of Glaciology* **3**(21), 33–38. doi: 10.3189/S0022143000024709.

Werder MA, Hewitt IJ, Schoof CG and Flowers GE (2013) Modeling channelized and distributed subglacial drainage in two dimensions. *Journal of Geophysical Research* **118**, 2140–2158. doi: 10.1002/jgrf.20146.

Zhao C and 11 others (2025) Subglacial water amplifies Antarctic contributions to sea-level rise. *Nature Communications* **16**(1), 3187–11. doi: 10.1038/s41467-025-58375-4.

Zoet LK and Iverson NR (2020) A slip law for glaciers on deformable beds. *Science (American Association for the Advancement of Science)* **368**(6486), 76–78. doi: 10.1126/science.aaz1183.

Downloaded from https://www.cambridge.org/core. 19 Nov 2026 at 14:02:16, subject to the Cambridge Core terms of use.